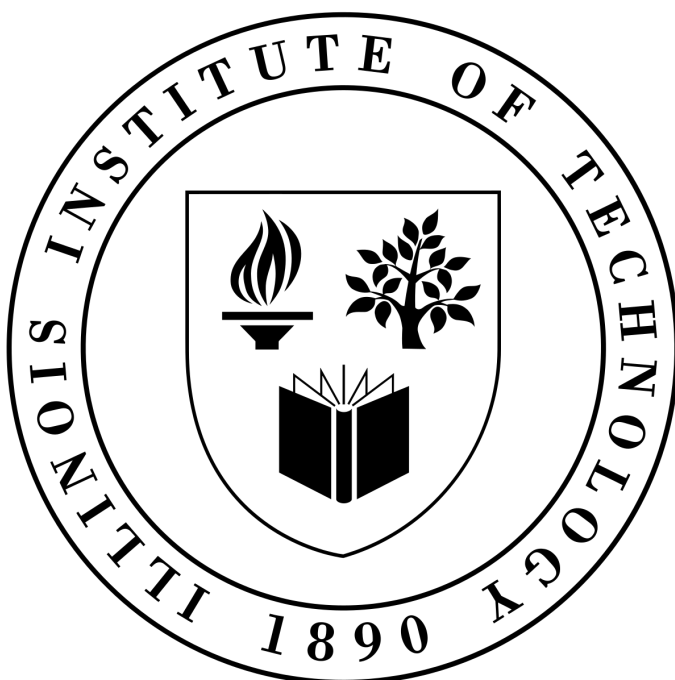


MMAE-414
AIRCRAFT DESIGN - GROUP THREE



IMT-22
PROJECT MORBIUS

PROJECT MORBIUS



ILLINOIS INSTITUTE OF TECHNOLOGY
ARMOUR COLLEGE OF ENGINEERING
MMAE-414 AIRCRAFT DESIGN REPORT
AIAA HYBRID ELECTRIC TURBOPROP

Project Morbius
October 20th, 2022

PROJECT MORBIUS

Team Structure

¹Eyob Ghebreiesus ²James Szewczyk ³Marek Jelen ⁴Matt Tobin

¹ M.Eng. Aerospace Engineering. Aerodynamics Lead. Deputy for Stability Control.

² B.Sc. Aerospace Engineering. Propulsion Lead, Deputy for Structures

³ M.Eng. Aerospace Engineering. Stability Control Lead, Deputy for Aerodynamics

⁴ M.Sc. Aerospace. Structures Lead, Deputy for Propulsion.

Homepage: *Project Morbius*

Created on *August 25th, 2022*

Published on *October 20th, 2022*

Copyright © 2022

All rights reserved. This Lab report or any portion thereof may not be reproduced or used in any manner whatsoever without the express written permission of the publisher except for the use of referencing for educational purposes.

The above copyright notice and this permission notice shall be included in all copies or substantial portions of the document.

Produced via LaTeX, Inc U.S.A.

MIT License for the GitHub Project, 2022

github.com/eyobghiday/project-morbius

Department of Mechanical, Materials and Aerospace Engineering

ILLINOIS INSTITUTE OF TECHNOLOGY

Contents

1	Introduction	1
1.1	Project Summary	1
1.2	Team Organisation	1
2	Mission Overview	1
2.1	Mission Requirements	2
2.2	Initial Sizing	2
2.3	Baseline Plane Dimension	5
3	Trade Study	5
3.1	Aspect Ratio and Wing Loading	5
3.2	T-W vs W-S Optimization	6
3.3	VN Diagram	6
4	Aerodynamics	9
4.1	Airfoil Selection	9
4.2	Main Wing	9
4.3	Flaps and Slats	10
4.4	Tail Configuration	11
4.5	Optimization	13
5	Propulsion	13
5.1	Hybrid Engine Configuration	13
5.2	Battery Sizing	15
5.3	Efficiencies	16
5.4	Integration	18
5.5	Engines	19
6	Stability & Control	19
6.1	Weight & Balance	19
6.2	Static Margin	20
6.3	Longitudinal Stability	20
6.4	Lateral Stability	21
6.5	Empty vs Full Weight	22
7	Structures	23
7.1	Material Selection	23
7.2	Fuselage	24

7.3	Landing Gear	24
7.4	CAD Drawing	24
8	Cost Analysis	30
8.1	2022 Adjustments	30
8.2	R&D Cost	31
8.3	Operation & Maintenance	31
8.4	Pricing and Revenue	32
9	Conclusion	32
9.1	Efficiency Merit	32
9.2	Conclusion	32
10	Appendix	33
10.1	Codes and Scripts	33
List of Figures		36
List of Tables		36
Abbreviations		37
References		37

1 Introduction

This report contains the conceptual design, analysis, and preliminary design of a hybrid engine turboprop aircraft. World renowned aircraft maker, Embraer released its most recent market outlook on turboprops and has estimated a demand for 1,080 turboprops around the world. This demand was seen to be led by Asia Pacific China, and US, with 490 aircraft allocated there [3]. Europe was the next largest segment, with 190 aircraft forecasted. For its own aircraft, due to enter into service in 2027-2028, it estimated demand of around 500 units alone from the company.

1.1 Project Summary

This project dubbed "IMT-22" short for It's Morbin Time 2022, is a hybrid turboprop aircraft designed for commercial air travel at an economic fare. Turboprop's generally strike a balance between the features of both piston-prop and turbojet airplanes. The specifications for this airplane design is carefully chosen, keeping with the guidelines proposed under the FAA 14 Part-25, ICOA Code-B and Code-C. This conceptual design report details each step of the design, analysis and optimizing process. Here the aerodynamic performances are explored, followed by stability, propulsion, and structural integrity to produce an optimal aircraft. The IMT-22 is expected to enter the market by 2035.

1.2 Team Organisation

The team is made of four members in total and their roles are shown in Table 4.1. Each role has a lead and a deputy that represent their significance and the tasks delegated.

Table 1.1 – Team Organization Chart

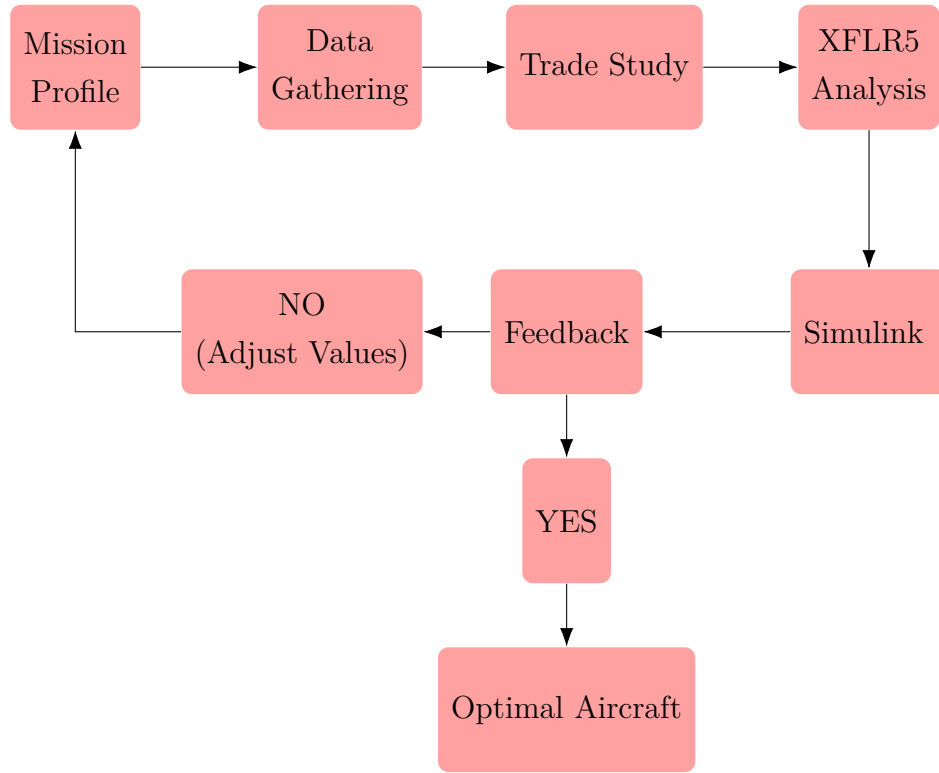
Subsystem	Lead	Deputy
Spokesperson	James Szewczyk	–
Aerodynamics	Eyob Ghebreiesus	James Szewczyk
Propulsion	James Szewczyk	Matthew Tobin
Structures	Matthew Tobin	James Szewczyk
Stability	Eyob Ghebreiesus	James Szewczyk
Cost Analysis	Marek Jelen	Eyob Ghebreiesus
Trade Studies	Eyob Ghebreiesus	James Szewczyk

2 Mission Overview

To ensure our project results in designing an effective and efficient aircraft, we have made a project plan to provide the best out put parameters in Figure 2.1. After initial mission definition, and requirements the project is closely followed by historical studies. Numerous data for existing turboprop aircrafts were collected firsthand. This data will be used to compare performance metrics of IMT-22 with existing planes. Once we select the design metrics like Aspect Ratio,

Take off Weight, Wing Loading, we use Python scripts, Initial sizing Matrix and other methods to graph the data and see where we land. After that we proceed into XFLR5 Airfoil analysis to test the values in the simulation. After reading the feedback from the simulation; if the findings are feasible, we proceed to component design phase. If not, we go back to refine our mission definition and operational requirements. This is an agile project managing system where we select the performance parameters and perceive the coverage, operation orbit and bypass simultaneously to decide the best fit. This allows us to be flexible with the little time provided.

Figure 2.1 – Project Flow



2.1 Mission Requirements

Our mission begins with developing new regional aircraft to satisfy the 50-seat portion of the market that meets the US domestic that has significantly better fuel burn and economics than existing options. The overall goal is to be at least 20% better than existing 50 seat regional turboprops in 500nmi block fuel per seat with a cost to build that is comparable to the existing aircraft, including the hybrid propulsion system. The specific requirements are listed below in Table 2.1.

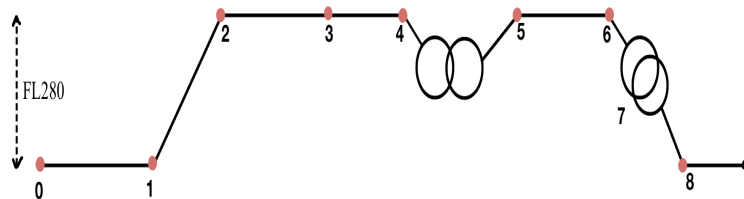
2.2 Initial Sizing

As per the requirements listed in Table 2.1, the team proceeded on to look at currently existing turboprops to understand their performances. In order to improve the efficiency of hybrid engines,

Table 2.1 – Specification Requirements

Requirements	Value
Passengers	50+/-4
Range (R)	1000nmi
Distance to Climb to Cruise Altitude	200nmi
Crew (2 pilots + 1 member)	3
Approach Speed (V_{app})	141KN
Min Cruise (V_{cruise})	275KTAS
Target Cruise (V_{cruise})	350KTAS
Max Takeoff Distance(S_{TO})	4500ft
Max Landing Distance($S_{Landing}$)	4500ft
Loiter Time	45min
Flying Altitude (FL280)	28,000ft
Pressurization Altitude	5,000ft
Min Seat Width	17.2in
Target Seat Width	18in
Max Wing Span (ICAO Code B)	78.8ft
Max Wing Span (ICAO Code C)	118.11ft
Carbon Reduction amount	20%
Entry Into Service (EIS)	2035
Certification Base	FAA-14 Part 25

and attain the required target, a mission profile is defined in Figure 2.2 to estimate weight fractions.

**Figure 2.2 – Mission Profile**

Where:

- 0 - 1: Engine Taxi/Takeoff
- 1 - 2: Climb
- 2 - 3: Cruise (Turbine Powered)
- 3 - 4: Cruise (Electric Powered)
- 4 - 5: Loiter (45m minute)
- 5 - 6: Diversion Cruise
- 6 - 7: Diversion Loiter (20 min)
- 7 - 8: Land

The mission profile accounts for additional diversion in case a first landing attempt is deemed impossible. It also serves as a safety factor, providing better aircraft analysis for commercial pur-

poses. The electric cruise section is placed at the end of the expected cruise segment to maximize range from the electric propulsion. The segment cannot be done before the diversion, as the crew would not have knowledge of the additional cruise section prior to the diversion.

Now that we have our mission profile, the weight fractions are calculated for each mission profile in Table 2.2. Note that since the aircraft is hybrid, some of the coefficients had to be adjusted instead of just using Raymer's values. A more detailed explanation of the electrical values is found in the Propulsion 5 section.

Table 2.2 – Mission Weight Fractions

Section	Fraction	Value	Notes
Taxi/Takeoff	$\frac{w_1}{w_0}$	1	Fully Electric
Climb	$\frac{w_2}{w_1}$	0.985	Raymer
Main Cruise	$\frac{w_3}{w_2}$	0.946	55.7% Turboprop Engine
Electric Cruise	$\frac{w_4}{w_3}$	1.00	44.3% Fully Electric
Loiter for Planned Landing	$\frac{w_5}{w_4}$	0.978	Raymer
Diversion Cruise	$\frac{w_6}{w_5}$	0.986	Breguet's Range
Diversion Loiter	$\frac{w_7}{w_6}$	0.99	Breguet's Endurance
Landing	$\frac{w_8}{w_7}$	1.00	Fully Electric
Hybrid Efficiency	η_{hyb}	0.91	Empirical
Fuel Mass Fraction	$\frac{w_f}{w_0}$	0.201	Multiplying Fractions

Data from current existing turboprop regional transports average a cruise SFC of 0.477. The SFC target is around 0.3816 lb/hr for cruise and an SFC of .32 for loiter. This SFC follows the expected increase in fuel efficiency of the recent Pratt and Whittney 127XT series turboprops. The 127XT series are already 18% more efficient than the current regional turboprop engines, with most using the PW150 series. With a 2% further increase in efficiency expected in the next decade, the SFC's targeted should be attainable before the 2035 delivery date.

$$SFC_{target} = 0.80 * SFC_{known} = 0.80 * 0.477 = 0.3816$$

From Raymer's Table 3.1, the empty weight fraction for a twin turboprop aircraft accounted for composite material structure (factor of 0.95) is:

$$\frac{W_e}{W_0} = 0.95 * 0.96 * W_0^{-0.05}$$

Now using Raymer's Equation 3.4, accommodating our battery and crew as total payload our estimated W_0 becomes:

$$W_0 = \frac{W_{crew} + W_{battery}}{1 - \frac{W_f}{W_0} - \frac{W_e}{W_0}} = \frac{12260 + 6288}{1 - 0.201 - 0.95 * 0.96(W_0)^{-0.05}} = 68343/lbf$$

With the mission weight fraction listed in Table 2.2 the summary of the calculated value is listed below.

Table 2.3 – Summary of Weights

Category	Note	lbf
Crew Weight	w_{crew}	660
Passenger Payload	w_{pass}	12000
Fuel Weight	w_{fuel}	13941
Battery Weight	w_{bat}	6288
Empty Weight	w_e	35723
Max Gross Takeoff	w_0	68343

2.3 Baseline Plane Dimension

Therefore our baseline plane dimension will be as shown in Table 2.4.

Table 2.4 – Baseline Plane Dimensions

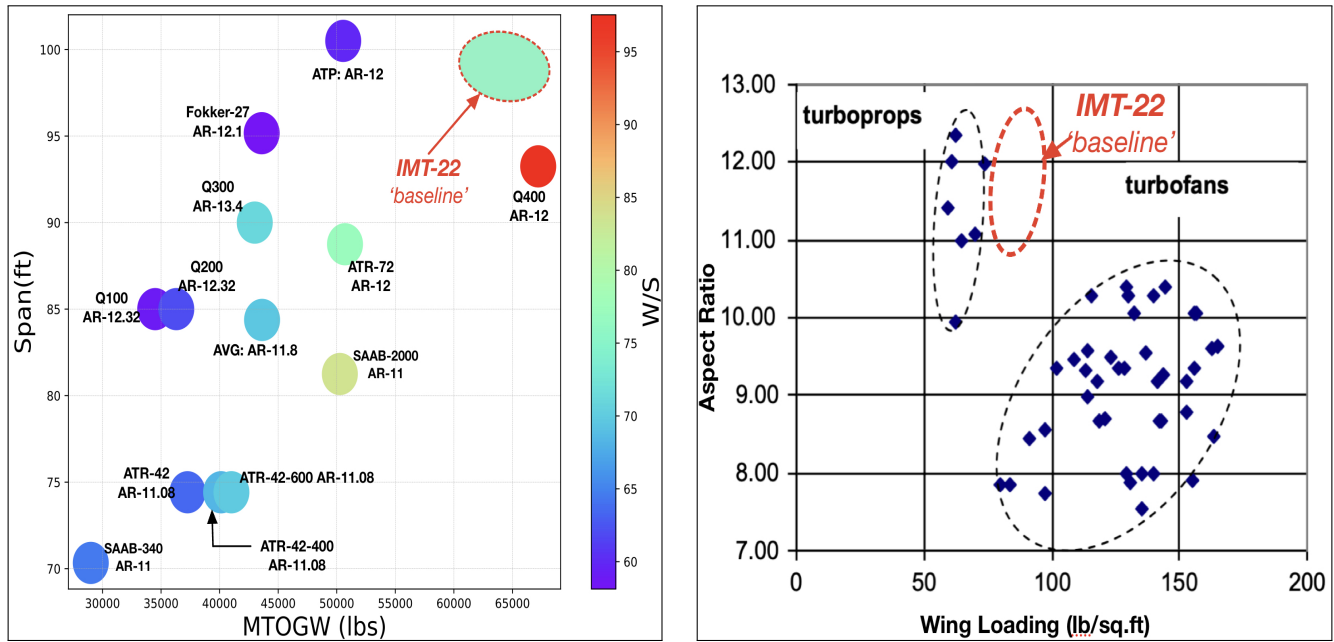
Category	Note	lbf
Crew Weight	w_{crew}	660
Passenger Payload	w_{pass}	12000
Fuel Weight	w_{fuel}	13941
Battery Weight	w_{bat}	6288
Empty Weight	w_e	35723
Max Gross Takeoff	w_0	68343
Aspect Ratio	AR	11.5
Thrust to Weight	$\frac{T}{W_0}$	0.205

3 Trade Study

3.1 Aspect Ratio and Wing Loading

It is known that Aspect Ratio greatly affects the wing loading and lifting capability. Aspect ratio is wing span divided by the wing area. But to determine the best AR (greater than 9 at least – Raymer [8]) we need to determine our wing loading. Raymer's Table 5.4 provides wing loading for turbo prop ($40 \frac{lbf}{ft^2}$), but those values are based on very old data and are low when compared to currently existing turboprops. First hand most older turboprops are flying at Mach=0.44, However the required cruise Mach for this design is 0.53-0.58 @ 28,000 altitude. Thus in order to meet the required specification we plotted *Span* vs W_0 to study the *Wingloading* for several existing turboprop planes (see Figure 3.1a). For the baseline maximum gross take off weight of $W_0 = 68343 \text{ lbs}$ and an AR of 12 we got around ($80 \frac{lbf}{ft^2}$) wing loading. This in return sets our wing span to be about $b = 102 \text{ ft} (30 \text{ m})$ or which is within the limits of ICOA Code-C requirement. This way we can relieve some of the wing loading (green shade) overhead without having to increase the

overall cost of the plane.



(a) $\text{Span vs } \frac{W_0}{S}$ against $\frac{W}{S}$. Red bar indicates the highest of wing loading in $\frac{\text{lbf}}{\text{ft}^2}$ for the displayed AR.

(b) Aspect Ratio of common existing turboprops and turbofans courtesy of Pasquale [9].

Figure 3.1 – Aspect Ratio and Wing loading

3.2 T-W vs W-S Optimization

Like Raymer said, the $\frac{T}{W}$ vs $\frac{W}{S}$ is the "granddaddy" of the trade studies [8]. For this design trade, the approach speed ($V_{app} \leq 141\text{kn}$), take off distance $S_{to} \leq 4500\text{ft}$ and fuel reduction $F_{red} \geq 20\%$ are used as constraints based on the report specification (see Table 3.1). The baseline highlighted in center is obtained from the initial trade studies, the rest are computed iteratively by varying the wing loading and thrust to weight values. Refer to the codes in the Appendix 10 section.

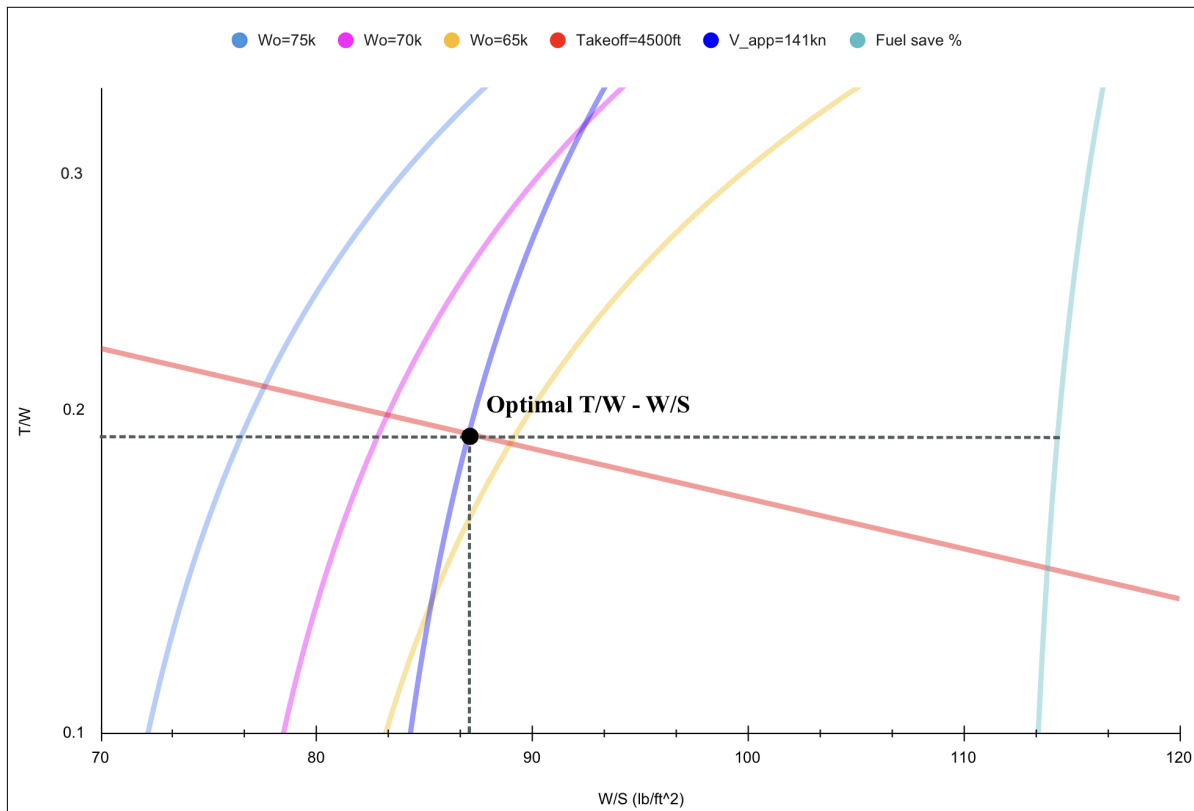
Now that we plot our design trade studies in Figure 4.3, the optimal combination of T/W and W/S is found from the intersection of the constraints. It shows that the initial estimation were shy away from the optimal values.

3.3 VN Diagram

The flight envelope defines operational limits for an aerial platform with respect to maximum speed and load factor given a particular atmospheric density. For the IMT-22 an aircraft cruises at 590ft/s (180m/s) as seen in the Figure 3.3. If it's flying anywhere outside the envelope lines it may suffer some structural damage, thus the limits should therefore never be exceeded. The blue dashed line represents the the limit of vertical gust load during cruise and the red dashed

Table 3.1 – Optimization Parameters

$\frac{T}{W} = 0.255$	$W_0 = 61419/lb$ $V_{app} = 130.0/kn$ $S_{to} = 2356/ft$ $F_{red} = 28.6\%$	$W_0 = 69752/lb$ $V_{app} = 137.7/kn$ $S_{to} = 2675/ft$ $F_{red} = 27.7\%$	$W_0 = 78086/lb$ $V_{app} = 145.7/kn$ $S_{to} = 2995/ft$ $F_{red} = 26.9\%$
$\frac{T}{W} = 0.205$	$W_0 = 60009/lb$ $V_{app} = 127.7/kn$ $S_{to} = 2961/ft$ $F_{red} = 20.8\%$	$W_0 = 68343/lb$ $V_{app} = 136.3/kn$ $S_{to} = 3372/ft$ $F_{red} = 27.8\%$	$W_0 = 76676/lb$ $V_{app} = 144.4/kn$ $S_{to} = 3783/ft$ $F_{red} = 27.0\%$
$\frac{T}{W} = 0.155$	$W_0 = 58612/lb$ $V_{app} = 126.2/kn$ $S_{to} = 4053/ft$ $F_{red} = 28.9\%$	$W_0 = 66947/lb$ $V_{app} = 135.0/kn$ $S_{to} = 4630/ft$ $F_{red} = 27.9\%$	$W_0 = 75279/lb$ $V_{app} = 143.1/kn$ $S_{to} = 5206/ft$ $F_{red} = 27.2\%$
	$\frac{W}{S} = 72 \frac{lb}{ft^2}$	$\frac{W}{S} = 82 \frac{lb}{ft^2}$	$\frac{W}{S} = 92 \frac{lb}{ft^2}$

**Figure 3.2 – Design Trade $\frac{T}{W} - \frac{W}{S}$**

line indicates the limit of vertical gust at dive speed.

Now that we have our optimal configuration listed in Table 3.2, we move forward to the detail

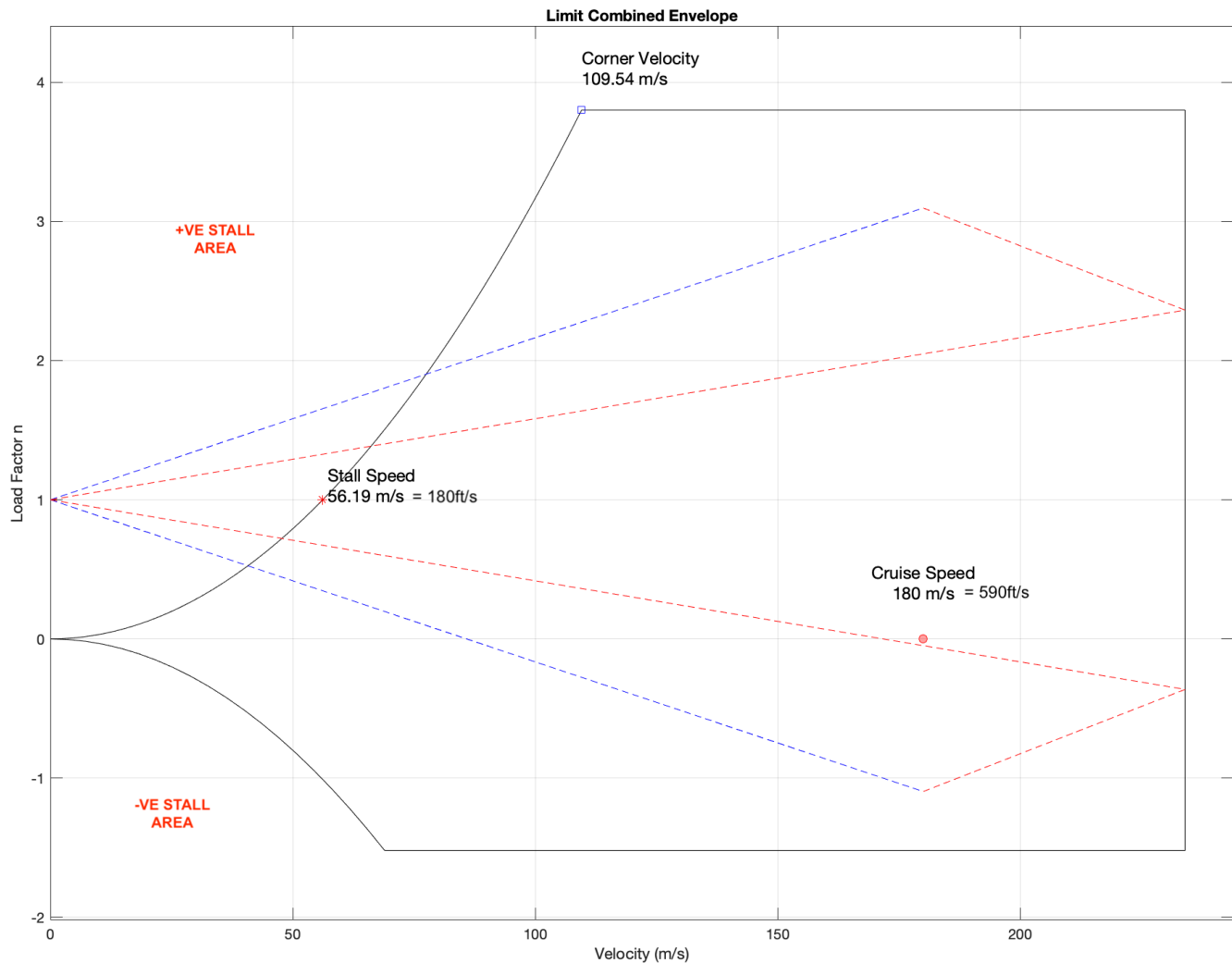


Figure 3.3 – V-n diagram)

design phase.

Table 3.2 – Optimal Plane Configuration

Category	Notation	Unit	$\pm\%$ error
Crew Weight	w_{crew}	660 lb	$\pm 2\%$
<i>Passenger Payload</i>	w_{pass}	12000 lb	$\pm 3\%$
Fuel Weight	w_{fuel}	13941 lb	$\pm 3\%$
Battery Weight	w_{bat}	lb	$\pm 1\%$
Empty Weight	w_e	35723 lb	$\pm 3\%$
Max Gross Takeoff	w_0	68000 lb	$\pm 2\%$
Wing Loading	$\frac{w_0}{S}$	$86 \frac{lb}{ft^2}$	$\pm 4\%$
Aspect Ratio	AR	12	
Wing Span	b	97 ft	$\pm 5\%$
Thrust to Weight	$\frac{T}{W_0}$	0.18	$\pm 1\%$

4 Aerodynamics

4.1 Airfoil Selection

The airfoil selected for the proposed design depends upon the cruising speed, which in turn is related to the powerplant chosen. The target V_{cruise} is 350kts ($Mach = 0.53$) for this project. Sweepback is unnecessary in this speed range so aspect ratios can be high (≥ 10).

From Raymer's Equation 4.5 we get our Cl_{design} as:

$$Cl_{design} = \frac{1}{q} * \frac{W}{S} \approx 0.2 \quad (4.1)$$

Additionally from Raymer[8] Figure 5.3 our maximum lift coefficient for a single slotted flap is about $CL_{max} = 2.1$. Therefore, the $Cl_{design} = 0.2$ multiplied by 10 tells us our airfoil number. The third digit starts with 2 and the last couple of digit's possible between 15-18% as a the root airfoil. Based on those values We narrowed down the list of airfoils to NACA 6-series and NACA-4 series for this aircraft. The NACA 6-series have smaller leading edge radii than the NACA 4-series and the NACA 5-series airfoils [9]. Keep in mind that due to XFLR limitation these airfoils are selected based on analysis of $Re = 9 * 10^6$ for XFLR.

Table 4.1 – Aifoils Considered

44XX	63XXXX	64XXXX
NACA-4415	NACA-63(3)218	NACA-64(2)415

It is recommended that the airfoil selected be chosen both on the value of Cl_{max} and upon the post stall variation of cl with angle of attack. An abrupt drop in section lift coefficient is to be avoided, and the airfoil with the smallest decrease in Cl for angles of attack above the stall is highly desirable, even at the expense of a smaller value of Cl_{max} .

Therefore NACA-63218 is the suggested airfoil section for the main wing because of its favorable stall characteristics.

The maximum thickness of the 4- and 5-digit airfoils is at 30% chord. The position of the maximum thickness of the 63, 64, and 65 series is located progressively aft. The 63 series airfoils might be considered for the turboprop aircraft. It is also possible to investigate those airfoil sections used by the competition (market survey aircraft) to aid in justifying the choice of airfoil.

4.2 Main Wing

For turboprops, a simple and efficient wing geometry is preferred [8]. Tapered wing generally have closer efficiency (78-80%) to that an elliptic wing (85%). Main factors that needed consideration were the Lift, Engine height clearance (turboprop) and ease of manufacturing. A typical trape-

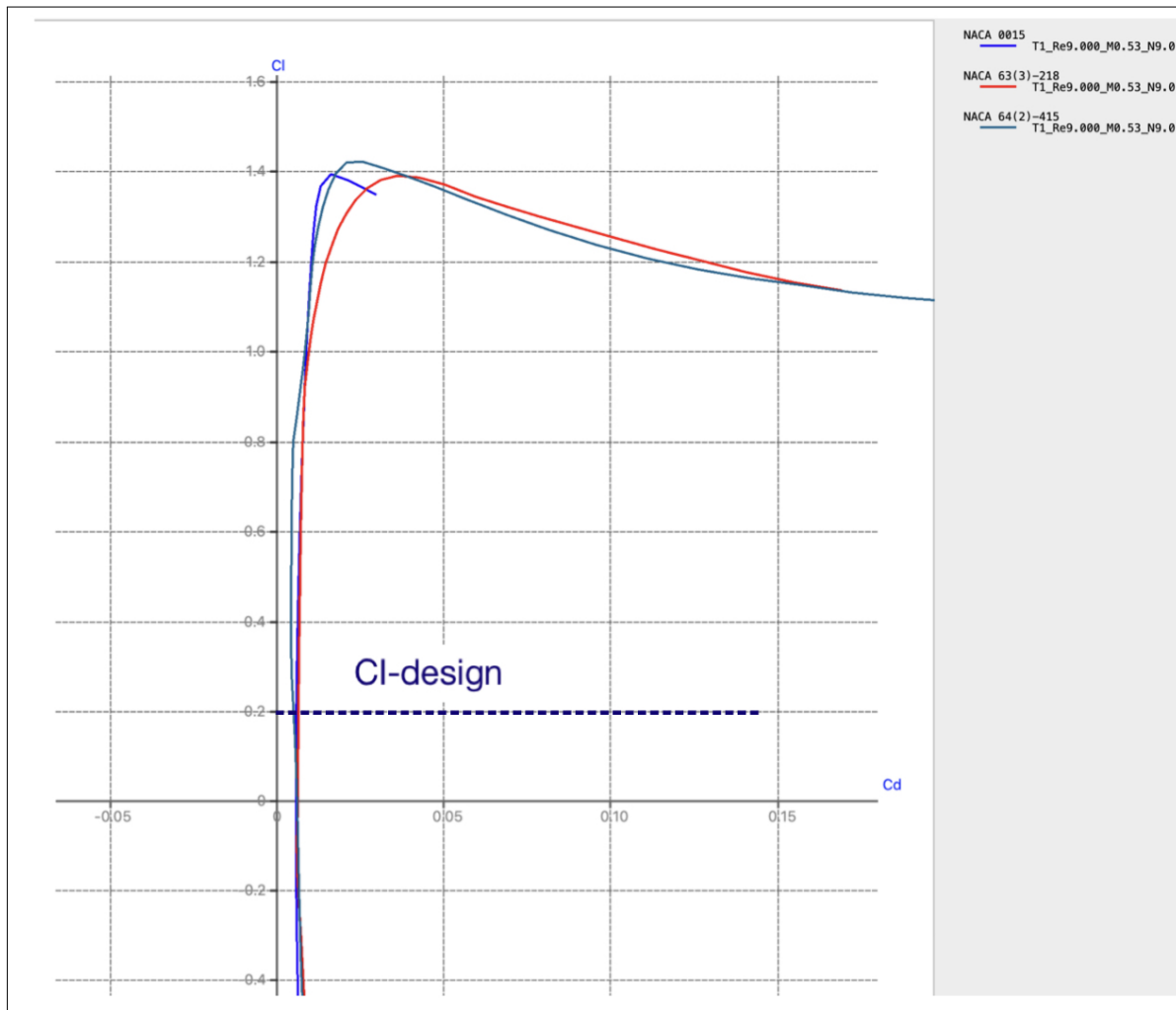


Figure 4.1 – C_l . vs. C_d at design Limit

Zoidal plan form requires the wing root and tip have different airfoil sections. This is because thicker airfoils at the root are necessary to accommodate the high wing root bending moment. On the other hand the tip airfoil thickness can be reduced for better airfoil performance due to much lower bending moments. Since there is no twist, the amount of lift produced by each wing section will be proportional to the chord length keeping the aircraft stable and steady. Additionally, the wing will have a dihedral angle of $\Gamma = 4$ to factor in the stability of the aircraft about the roll axis. Table 7.1 shows the summary of our tapered wing dimension.

4.3 Flaps and Slats

IMT-22 will utilise a slotted flap. Typically the flap depth c_F amounts to about 30% of the chord. The slotted flap increases lift by increasing the airfoil camber. Ailerons, elevators and rudders will be slotted flaps for this aircraft. This setting would accommodate the slightly small C_l values to about $CL_{max} = 2.1$ hitting that required high lift during landing and takeoff.

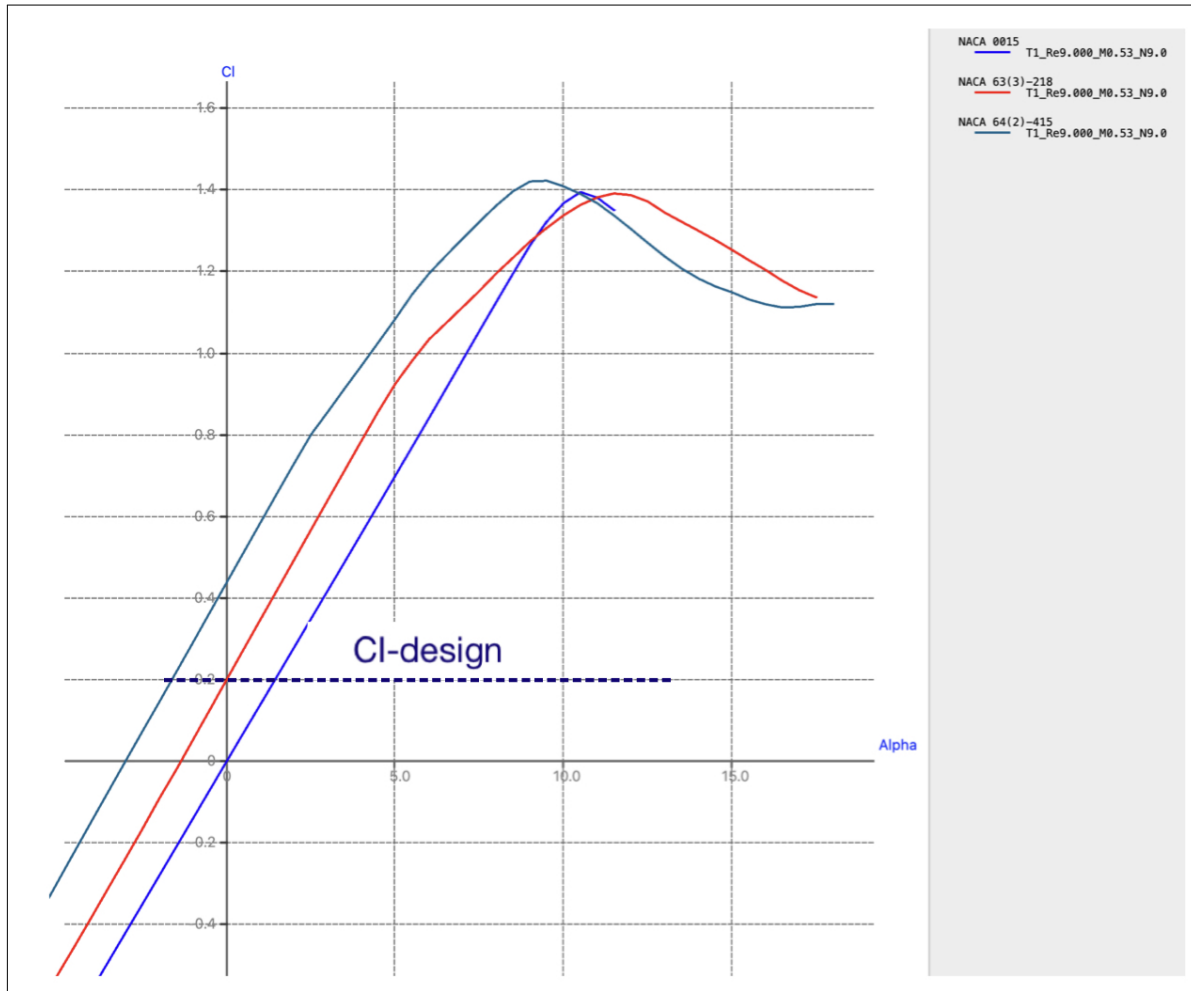


Figure 4.2 – C_l . vs Alpha

Table 4.2 – Wing Specification

Parameter	Value	Parameter	Value
Root Airfoil	NACA: 63(3)-218	Aspect Ratio (AR)	12
Root Airfoil	NACA: 63(3)-215	Taper Ratio (λ)	0.45
Span (b)	100.2ft	Dihedral Angle (Γ)	4-deg
Root Chord	11.2ft	Sweep Angle (δ)	0
Tip Chord	5.04ft	Max $\frac{t}{c}$	24%
Total Area	790ft ²	X_{Loc}	37

4.4 Tail Configuration

Four different tail configurations were considered for this aircraft. Stability, Ease of Manufacture and drag. Table 4.3 is a selection matrix that compares each of this based on weights. T-Tail's greatest advantage is keeping the elevators out of the disturbed airflow from the wing and fuselage. This also allows for improved glide ratio.

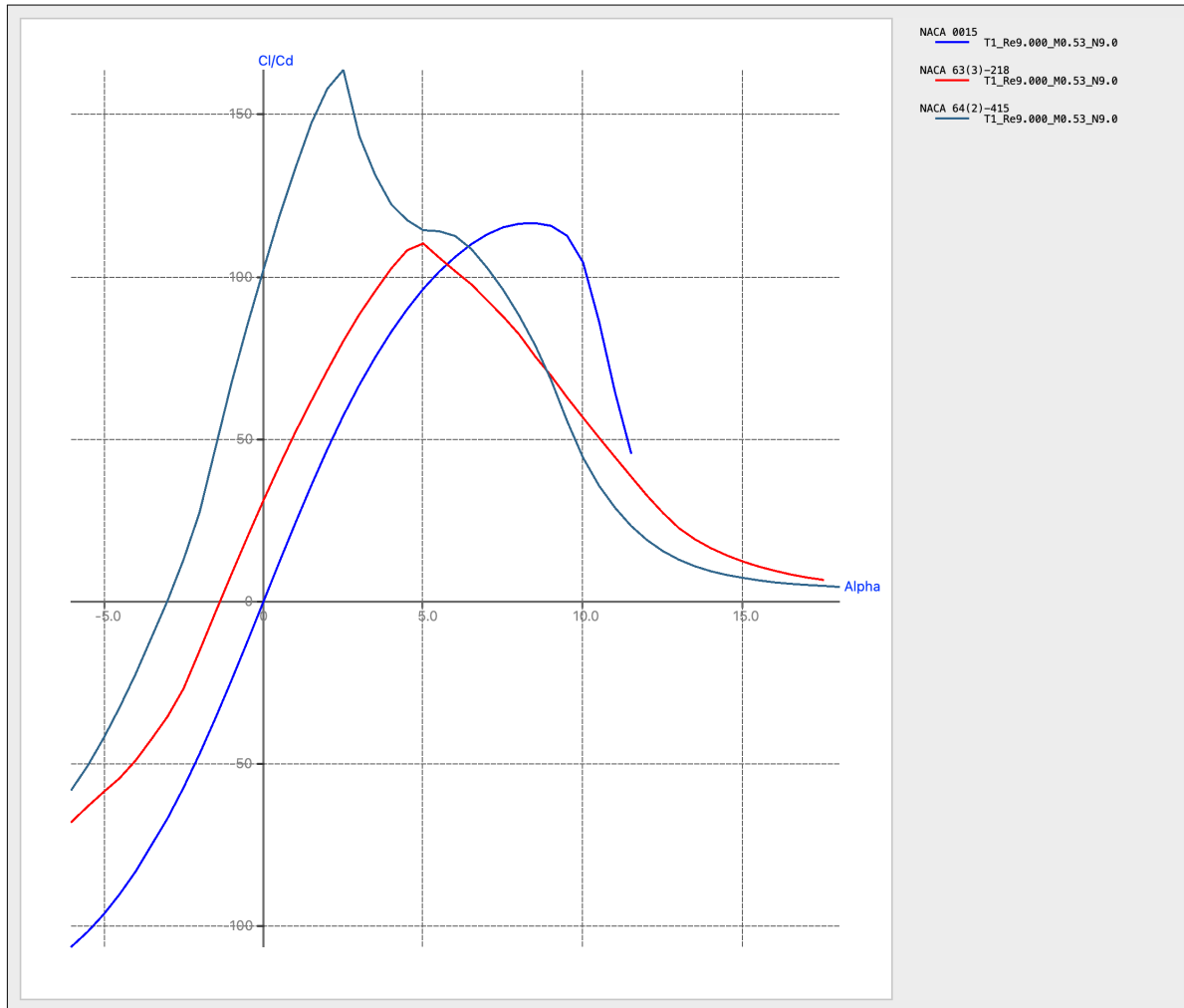


Figure 4.3 – Cl/Cd vs. α

Table 4.3 – Tail Configuration Matrix

Criteria	Weight	V-Tail	H-Tail	T-Tail	Conventional
Manufacturing	20	1	3	4	3
Stability	30	1	4	3	2
Drag	50	4	1	2	1
Total	100	250	250	270	170

For both Horizontal tail NACA0012 airfoil has been chosen. For vertical tail NACA0015 airfoil has been chosen.

4.4.1 Horizontal

Summary of the Horizontal Tail:

Table 4.4 – Horizontal Tail

Parameter	Value	Parameter	Value
Root Airfoil	NACA-0012	Aspect Ratio (AR)	5.4
Tip Airfoil	NACA-0012	Taper Ratio (λ)	0.6
Span(b)	26.25ft	Incidence Angle (Γ)	-1.5
Root Chord	6.1ft	Sweep Angle (δ)	0
Tip Chord	3.66ft	Max $\frac{t}{c}$	12%
Total Area	127.97ft ²	X_{Loc}	55.8ft

4.4.2 Vertical

Similarly below is a summary of the vertical Tail:

Table 4.5 – Vertical Tail

Parameter	Value	Parameter	Value
Root Airfoil	NACA-0015	Aspect Ratio (AR)	3.9
Tip Airfoil	NACA-0015	Taper Ratio (λ)	0.6
Span(b)	14.76ft	Dihedral Angle (Γ)	0
Root Chord	9.343ft	Sweep Angle (δ)	0
Tip Chord	5.7ft	Max $\frac{t}{c}$	15%
Total Area	111.0ft ²	X_{Loc}	56.2ft

4.5 Optimization

5 Propulsion

5.1 Hybrid Engine Configuration

For the hybrid powertrain, there were 2 configurations analyzed to integrate the hydrocarbon and electrical propulsion systems. These options were:

Series: In a series system, the engine is connected to a generator rather than being directly connected to the driveshaft. This generator is used to power a single electric motor, with additional power supplied by a main battery. The battery can also be charged directly through the generator. A series system offers distinct efficiency advantages by allowing the turboprop engine to run at its highest efficiency at all times and using electrical motor to augment the power required. The series system is also a simple design that requires little additional development to adapt current engine technology[1]. However, the addition of a generator reduces the efficiency of the system. The series system is shown in 5.1.

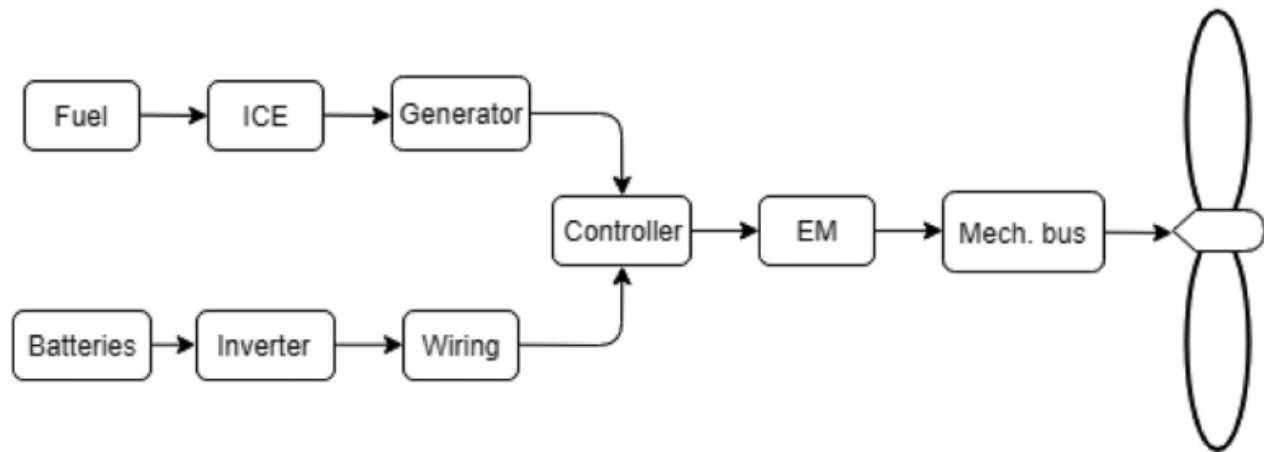


Figure 5.1 – Series Powertrain

Parallel: A parallel system uses a single gearbox to mate both the electric and turboprop shafts to rotate one shared driveshaft that drives the propeller[1]. The parallel system is safer than the series configuration in the event of a single motor / engine failure, as well as more efficient than the series configuration. Parallel systems are more complex, and louder than series configurations. The parallel system is shown in 5.2.

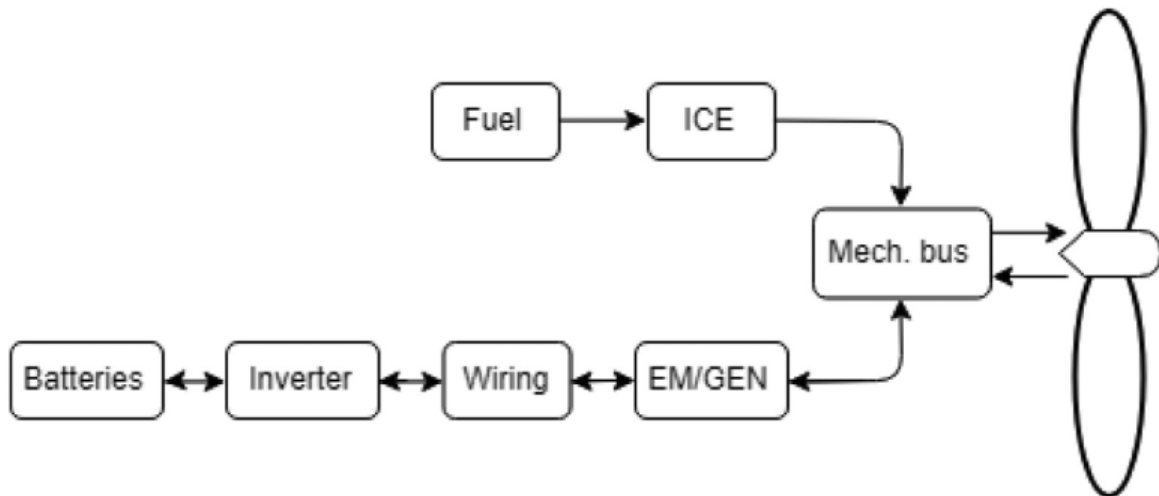


Figure 5.2 – Parallel Powertrain

Distributed: A distributed system uses a separate hydrocarbon system as well as an electrical system. Distributed hybrid systems are most similar to conventional hydrocarbon aircraft, as the electrical system is completely isolated from the engines. This is the heaviest, but simplest configuration.

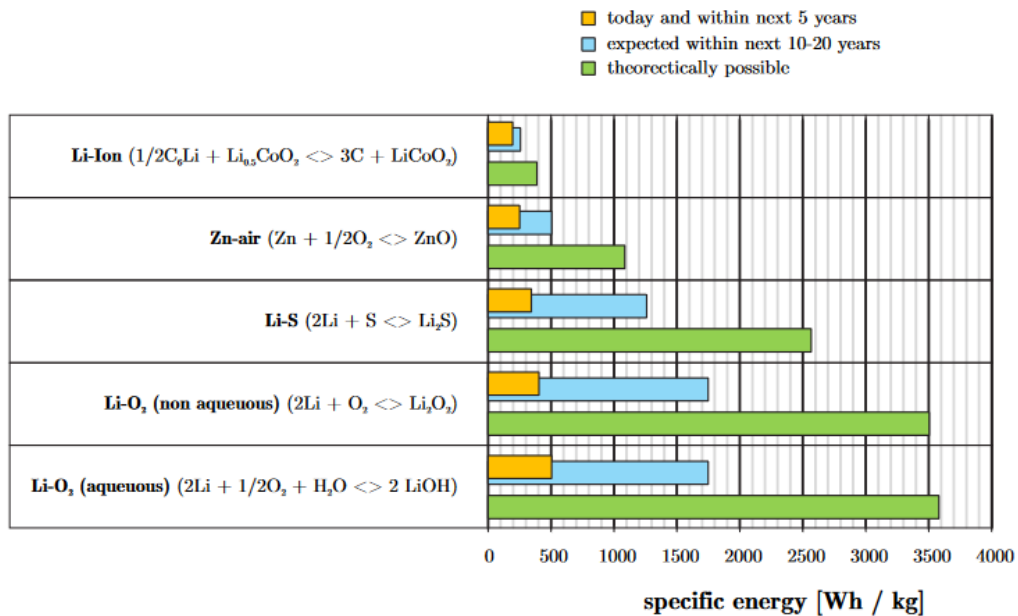
The selection matrix shown below was used to determine the configuration used for the aircraft.

Table 5.1 – Propulsion Selection Matrix

Criteria	Weight	Series	Parallel	Distributed
Complexity	20	2	1	3
Efficiency	45	2	3	1
System Weight	35	3	2	1
Total	100	235	225	140

5.2 Battery Sizing

To size the battery, the gravimetric energy density of the battery must first be estimated for the production year of 2035. The current energy density of cutting edge Lithium-Ion batteries is 245 kilowatt hours per kilogram. In 2035, using the Hepperle 2012 energy report [4], the energy density of the best option available was pessimistically estimated to be $1050 \frac{kW\cdot h}{kg}$ using Lithium-Sodium batteries.

**Figure 5.3 – Predicted Energy Density of Battery Types**

The battery was sized by estimating the amount of energy required to power the aircraft for 30 minutes on electric power only. Using Table 5.2 from Raymer, the power to weight for the aircraft was estimated to be $0.20 \frac{hp}{lb} = 14000 \text{ hp}$. Using the following equations, the mass of the battery was calculated.

$$M_{batt} = \frac{Pt}{e_{sb}\eta_{prop}} = 6288 \text{ kg} \quad (5.1)$$

For electric aircraft, Brequet's Range equation can be re-derived to be:

$$R = 3.6 \frac{L}{D} \frac{e_{sb}\eta b 2s\eta_p}{g} \frac{w_b at}{w} \quad (5.2)$$

Using this equation, the additional range provided by the battery can be estimated. When initially sizing the aircraft, this equation was also used to attempt to find a battery mass fraction (BMF) to see if the mission could be done with electric power alone. The BMF was found to be over 60%, and with any reasonable empty weight fraction, this would not be valid.

From the electric range equation, as electric flight does not result in a loss of mass, the range from electric flight can be optimized by using the electric system as late as possible in the planned trip. As a result, our cruise estimates were broken up into two cruises:

Normal Cruise: The first section uses the turboshaft engines to power the generator. The power from the generator is then immediately used to power the electric motors.

Electric Cruise: This section uses only the energy stored in the battery to cruise. This section should always be done as late as possible in the mission to optimize efficiency.

With the current version of the aircraft, the electric cruise distance of the aircraft is 212 nmi when done at the end of the normal cruise section.

5.3 Efficiencies

The mandatory efficiency requirement is a fuel reduction of 20% over the duration of a 500 nmi mission. All efficiencies used in this section describe the equivalent reduction in fuel used. The sources of efficiency identified were:

Engine Advancements Current turboprops use 1970's and 80's engines and have not seen the level of research as turbofan technologies. This can partially be contributed to the monopolization of the turboprop engine segment by Pratt & Whitney, who make 98% of the current civil aviation turboprop engines. However, Pratt and Whitney have developed the 127x series, with an engine in our horsepower class in production by 2025. The 127x series claims a SFC reduction of 18% when compared with the current PW150 series. Approximating another 2% in SFC reduction in the 13 additional years until production, the fuel savings from the usage of updated engines was estimated to be 20%.

Our aircraft would also be a suitable candidate for propfan or open rotor style engines, should the technology ever come to market. With the higher bypass ratio and thrust promised in comparison to turboprop engines, the aircraft is in the correct weight class to benefit the most from this area of research. The additional cabin noise and vibrations would be areas of concern on this new design.

Regenerative Braking Much like the similar technology employed in electric vehicles, the rotational inertia of the propeller can be turned back into usable energy via the electric motor. The current estimates of regenerative braking efficiency is 70% energy recapture.

Regenerative braking can be used during taxi and descent phases to minimize energy usage. During descent and landing, the aircraft can utilize a low regenerative strength during the descent glide or propeller windmilling to recapture some of the energy for the next mission. This comes with the added benefit of taxing and descending only under electric power, further reducing the mass fuel fraction required. Additionally, like the 787, regenerative braking is used on the electric braking system. This form of braking is mostly used for weight savings and reliability, but in theory could result in a very small regeneration. The energy recoverable from the descent phase assuming a 5% net energy recovery is shown below:

$$U = mgz = 45000 * 9.8 * 10668 = 4.7GJ = 1306kWH \quad (5.3)$$

$$E_{poten} = U * 0.05 = 59.591kWH \quad (5.4)$$

Conversion Inefficiencies: Conversion of the turboshaft energy into electrical energy requires a generator, inverter, and wiring which all require an efficiency loss. The equation for the hybrid efficiency is shown in Equation 5.5.

$$\eta_{hyb} = \eta_{gen}\eta_{invert}\eta_{wiring} = 0.912 \quad (5.5)$$

This efficiency must be applied to all fuel-burning stages of flight, resulting in an efficiency loss of approximately 9%. This may improve before 2035, as significant work is being done to improve inverter efficiency and improving generator integration. Supercooling has been proposed to improve generator efficiency to over 99.99%, but this requires the storage of unstable and complex liquid hydrogen storage unsuitable for an aircraft of this size and needed reliability.

The overall efficiency of the aircraft was measured using the equation below using the efficiencies outlined in this section, as well as accounting for the lack of fuel used during electric cruise, taxi, and descent.

$$\%f_{reduced} = \eta_{desc} + \eta_{taxi} + \eta_{wf} + \eta_{cruise} + \eta_{motor} - \eta_{hyb} = 0.276 \quad (5.6)$$

5.4 Integration

Using a series configuration, there are two potential options for electric motor placements and sizes. A "rubber motor" large electric motor can provide the power needed similar to a conventional twin turboprop. A turboshaft engine is placed behind this motor in the nacelle to power the motor and recharge the battery. This configuration has the advantage of simplicity and convention, though it is heavier and more complex than a conventional twin turboprop. The electrical efficiency of such a large motor would also be quite poor. This configuration was chosen to allow for usage of historical data from existing twin turboprops.

The second configuration is a distributed style system, with the leading edge of the wing supporting 20 or more small electric motors[1]. These smaller motors offer better power to weight, efficiency, and thermal characteristics when compared with a single large motor. The large quantity of motors also improves reliability in the event of a motor failure. However, the faster spinning small propellers make this method unsuitable for a 350 knot cruise speed, as the propeller tip exceeds the speed of sound. This distributed system is better suited for high endurance aircraft and low speed applications. There is likely a compromise with 4-8 medium size motors, though this optimization is quite difficult without historical data for similar sized electric aircraft.



Figure 5.4 – A Conceptual Distributed Electric Regional Aircraft

5.5 Engines

There were two engines of consideration for our power requirement of 6000-7000 ESHP per engine, the Pratt and Whitney PW150 and the Honeywell T-55-GA-715 [7]. The PW150 is the only civil option available, as this T-55 variant is for military applications only. Additionally, there would need to be adjustments to the PW150 to convert to a turboshaft version.

Table 5.2 – Engine Options

Engine	ESHp	TSFC	Weight (lbs)
PW150	6200	.43	1521
T-55	6500	0.49	830

As mentioned in the Efficiencies section, the best candidate for the turboprop engines is the PW127x 6000+ hp variant that has not yet been produced [6]. The lowered SFC and weight will greatly improve performance, but the details of this mystery engine are unknown outside of the horsepower range, SFC target, and planned introduction in 2025. This would likely be our engines for the aircraft, or a comparable propfan design. The engines selected for the aircraft were initially sized to be 7050 hp each, for a total ESHP of 14,100 hp total. This estimate was based off of the Raymer value of $0.20 \frac{hp}{lb}$ for twin turboprop aircraft. The 4-blade propeller was then sized to be:

$$D = K_p P^{1/4} = 1.5(7050^{1/4}) = 9.16\text{ft} \quad (5.7)$$

6 Stability & Control

6.1 Weight & Balance

In order to obtain accurate stability, we need to accommodate all the component weights to a greater degree. A summary of weights and balances sheet is listed in 6.1 below. Distances are with $x = 0$ at the leading edge of the wing.

Table 6.1 – Weights and Balances Sheet

Category	X _{Loc} (ft)	Mass (lbs)
Empty Wing	3.9	5240
Horizontal Tail	57.9	3400
Vertical Tail	56.3	3600
Fuselage	-2.4	7907
Crew Weight	-28	660
Passenger Payload	5.0	12000
Fuel Weight	3.85	13941
Battery Weight	-21.0	13973
Empty Weight	3.01	35723
Max Gross Takeoff	3.29	68343

Passenger CG and Fuel CG were intentionally located close to the quarter chord of the main wing to minimize the change in $\frac{C_m}{\alpha}$ due to the usage of fuel or low passenger quantities. The engine masses were also placed at the same Z as the CG to align the center of thrust with the CG. The model used for stability analysis is shown in 6.1.

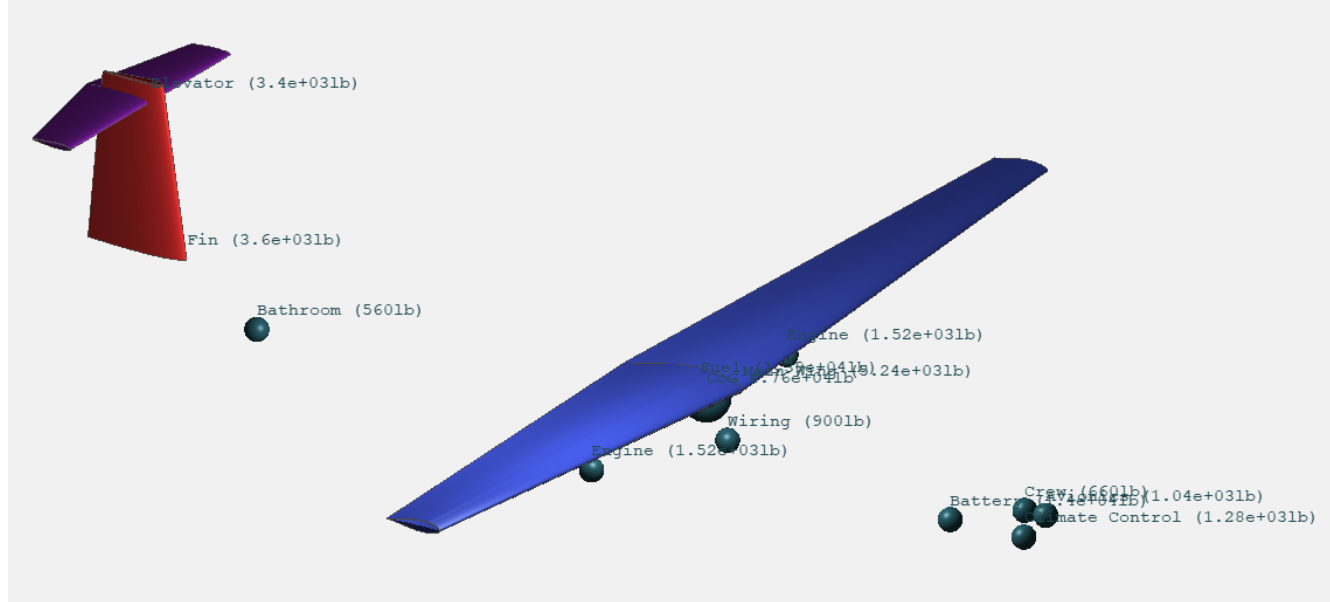


Figure 6.1 – XFLR Plane with Masses

6.2 Static Margin

The static margin can be found from the equation:

$$SM = \frac{X_{NP} - X_{CG}}{C_{MAC}} * 100 = \frac{6.099 - 2.908}{8.509} * 100 = 37.4\% \quad (6.1)$$

This static margin is quite high, indicating a low level of maneuverability. This is desirable for a civil transport aircraft, but this if the plane is found to be too unresponsive, the angle of incidence of the main wing or elevator can be changed. The elevator incidence for these tests was at -1.5 degrees.

6.3 Longitudinal Stability

Preliminary aircraft CG was placed at the quarter chord location of the main wing plus 5 feet. Analysis was then run to determine trim angle by visually confirming a negative slope C_m vs α and a positive trim angle between 2.5 - 4 degrees.

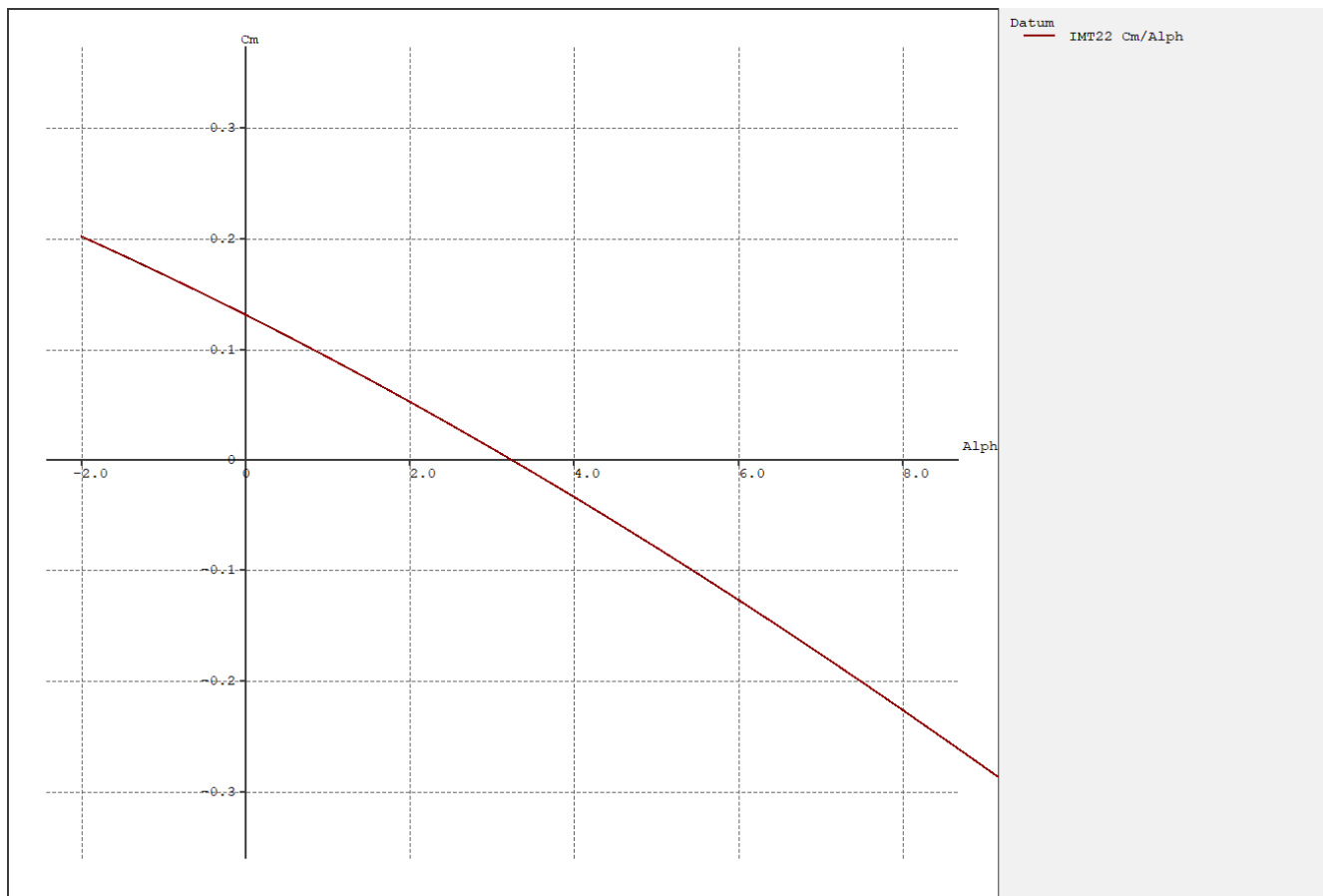


Figure 6.2 – Cm vs. Alpha for the Max Takeoff Weight

The trim angle for the aircraft at maximum takeoff weight was 3.28 degrees.

6.4 Lateral Stability

To determine directional stability, a Type 5 analysis can be used to plot C_n vs Beta and examine the slope. A stable aircraft will have a $\frac{dC_n}{d\beta} > 0$, implying a restoring yaw moment.

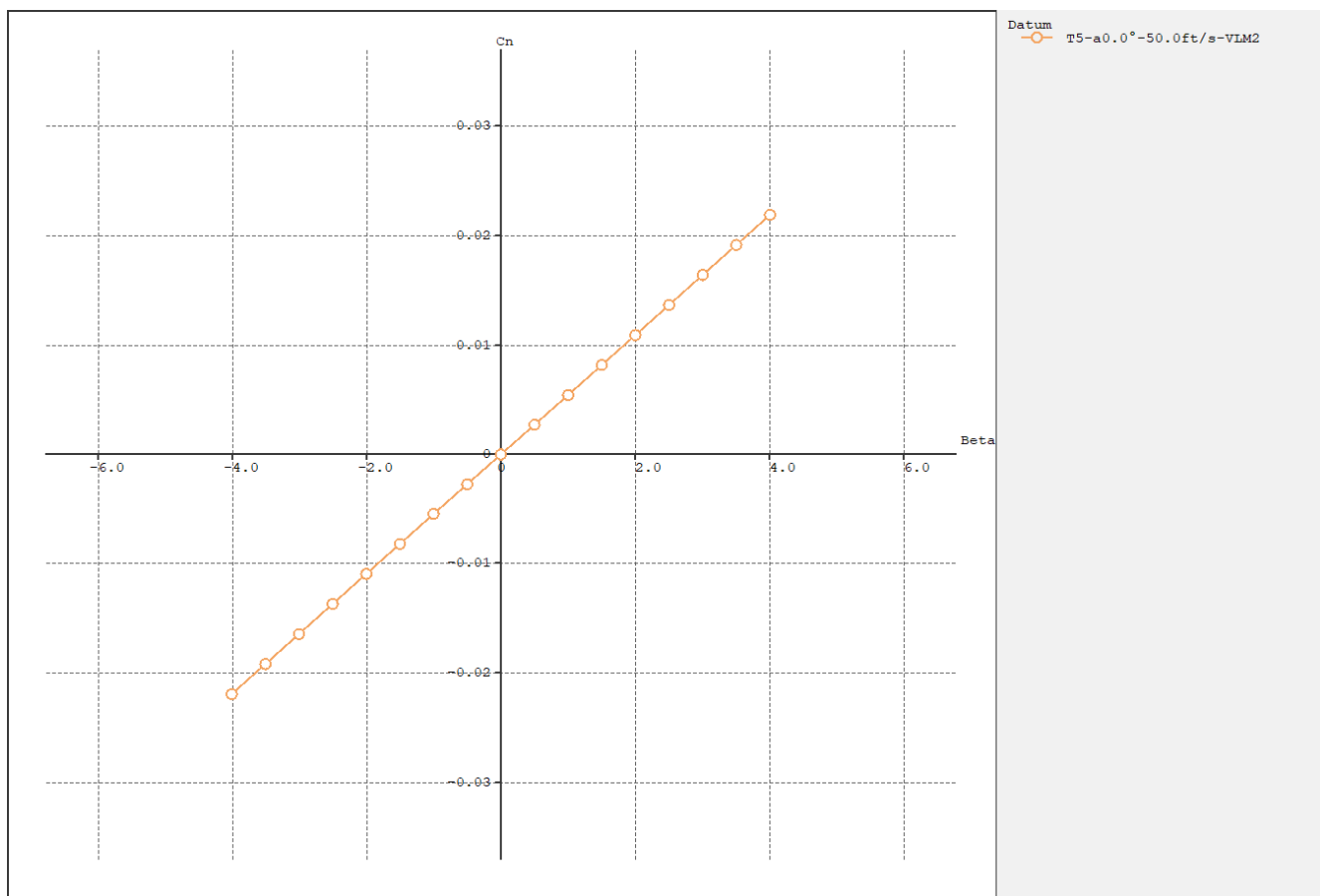


Figure 6.3 – C_n vs. β for the Max Takeoff Weight

The slope $\frac{dC_n}{d\beta}$ was found to be 0.0053, implying the aircraft is directionally stable.

To examine lateral stability, a stability analysis T-7 VLM2 can be used to determine if $\frac{dC_l}{d\beta}$ would be positive. Unfortunately, due to the Reynold's number limitation this analysis cannot be run for this size and speed of aircraft. The maximum Reynold's number found to function was 9,000,000. However, to run the T-7 analysis, a Reynold's number of 13,000,000 is required for the root airfoil. This technical issue has resulted in an inability to examine lateral stability for now. If the analysis was successfully run, a negative $\frac{dC_l}{d\beta}$ would imply a stable aircraft. In the future, a scaled version of the aircraft may be used to attempt to run this analysis.

6.5 Empty vs Full Weight

During flight, the fuel weight will decrease as it is used, though the CG location can be constant by pumping fuel around. However, in the event of pure electric flight, the plane must still be stable without the mass of the fuel. Similarly, for lower capacity flights or transports, the aircraft must still be stable without passenger weights. To determine the empty stability, the longitudinal stability was examined for a no fuel case, a no passenger case, and a no fuel and no passenger case.

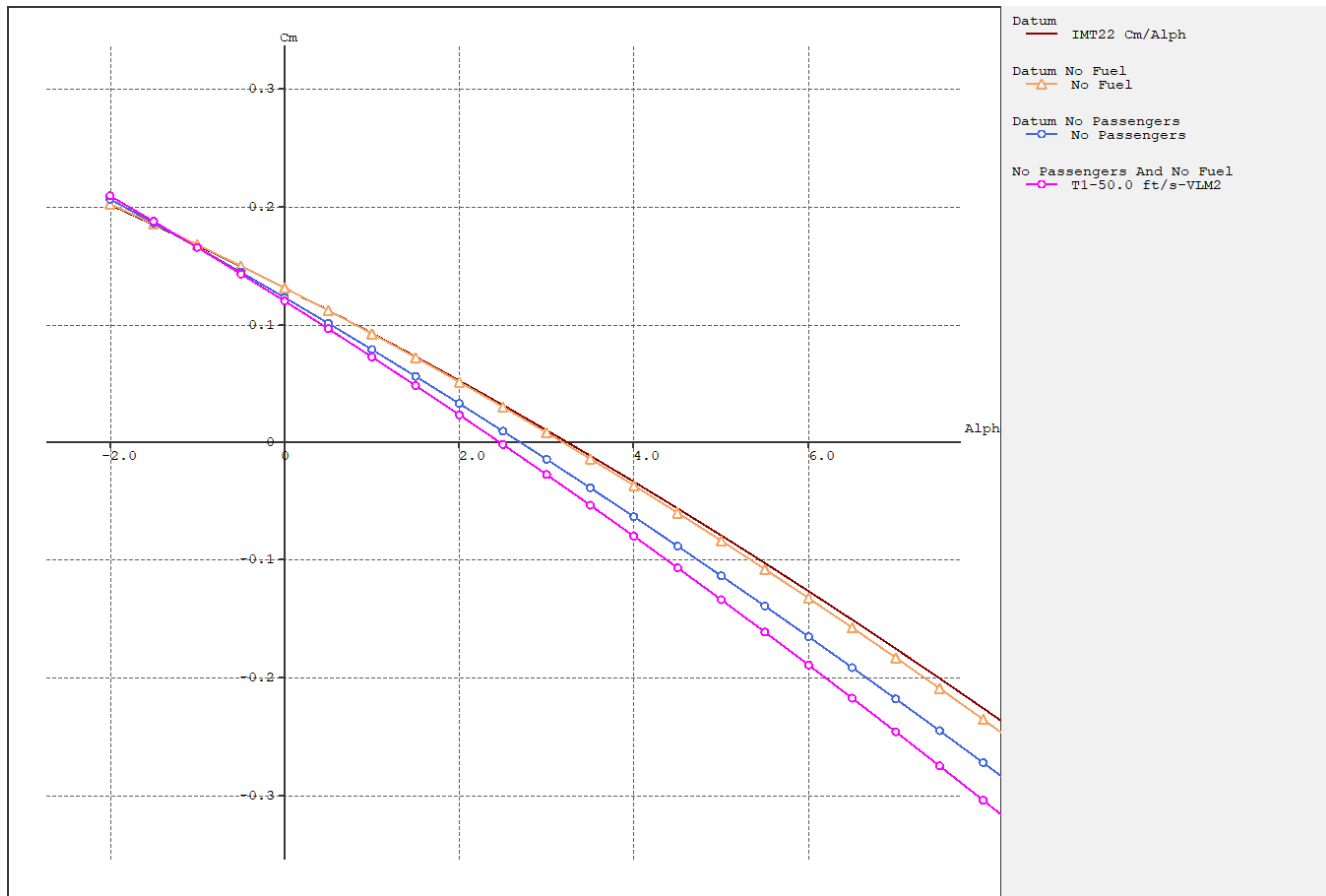


Figure 6.4 – C_m vs. α for Empty Weights

The trim angles were both lower for the empty cases, but still within acceptable ranges. The "no-fuel" case had a trim angle of 3.18 degrees, the "no-passenger" case had a trim angle of 2.70 degrees, and the "neither" case had a trim angle of 2.46 degrees. There is room for improvement through better organization of passenger seating and cargo, in addition to battery placement.

7 Structures

The structure of the airplane is one of the most important parts of an aircraft. It is what withstands all the aerodynamic forces as well as the stresses of the different varying weights on the plane, such as the passengers, wings and fuel. On top of all these, perhaps the most important aspects of the structure of an airplane, is that it makes sure that everyone gets to their destination in one piece by not breaking while in flight.

7.1 Material Selection

Materials can make or break an aircraft. Choosing the correct material for your aircraft will either make your plane famous on the news for a crash or not heard about at all because it never went down. With that being said, the material selection used for IMT22 can be seen in the Table 7.1. Table 7.1 was used to compare the properties of materials which allowed us to choose the

best material for each section of the airplane. This data can be found in Matweb.com [5]. After consideration of materials, it was found that using composite materials reduced our initial weight, w_0 , by 14%. This was one of the reasons we chose it. In addition to composite materials being lighter than traditional materials such as Al-6061, they are also better suited for aspects of the aircraft.

Table 7.1 – Material Selection

Material	Density (slug/in ³)	Young's Modulus (ksi)	Yield Strength (psi)	Tensile Strength (psi)	Elongation %
Fiberglass	4.831	10000	439900	439900	4.8
Carbon Fiber	3.394	5200	25000	15000	2
Al-6061	5.237	10000	7000	17000	25
Ti-6Al-4V	8.593	16500	160000	170000	10

7.2 Fuselage

The fuselage was designed to have the passengers and flight attendant be in the main section with an overhead luggage section for their carry-on luggage, extra compartments for storage, the lavatory, as well as the food and drink storage the flight attendant will be using. Under the main section is the undercarriage and this runs the length of the fuselage. This section will be used to hold checked in luggage as well as the main battery.

7.3 Landing Gear

The landing gear configuration we chose for our turboprop were tricycle landing gear. This is because it is the most common type of landing gear used for turboprop planes. Tricycle landing gear are used with turboprops because they have good ground stability and they allow for a flat cabin floor since our design is for a passenger airplane.

7.4 CAD Drawing

Many of the dimensions for the IMT22 came from using measurements and parameters outlined in Rayemer's book [8]. These parameters and measurements led to the design all the way from the fuselage, seating arrangement, passenger and flight attendant chairs to the design of the lavatory. Figures 7.1-7.5 show the CAD model and Figures 7.6-7.7 show CAD Drawings of the IMT22. The figures show the following:

Figure 7.1 shows a three-dimensional view.

Figure 7.2 shows a side view.

Figure 7.3 shows a front view.

Figure 7.4 shows top view.

Figure 7.5 shows a three-dimensional view with the plane cut right down the middle, the x-z plane, so that the following can be seen: half the passenger's seating arrangement, flight attendant's seat, lavatory (located on back of plane), the cockpit, the emergency exit, as well as the undercarriage.

Figure 7.6 shows the CAD drawing with some of the following dimensions: Wingspan of the Main Wing, Vertical Wing and Horizontal Wing, the length of the Fuselage, as well as the length from leading edge of the Horizontal Wing to the leading edge of the Main Wing.

Figure 7.7 shows the CAD drawing that describes the layout and dimensions of the seats for the passengers as well as the aisle length.

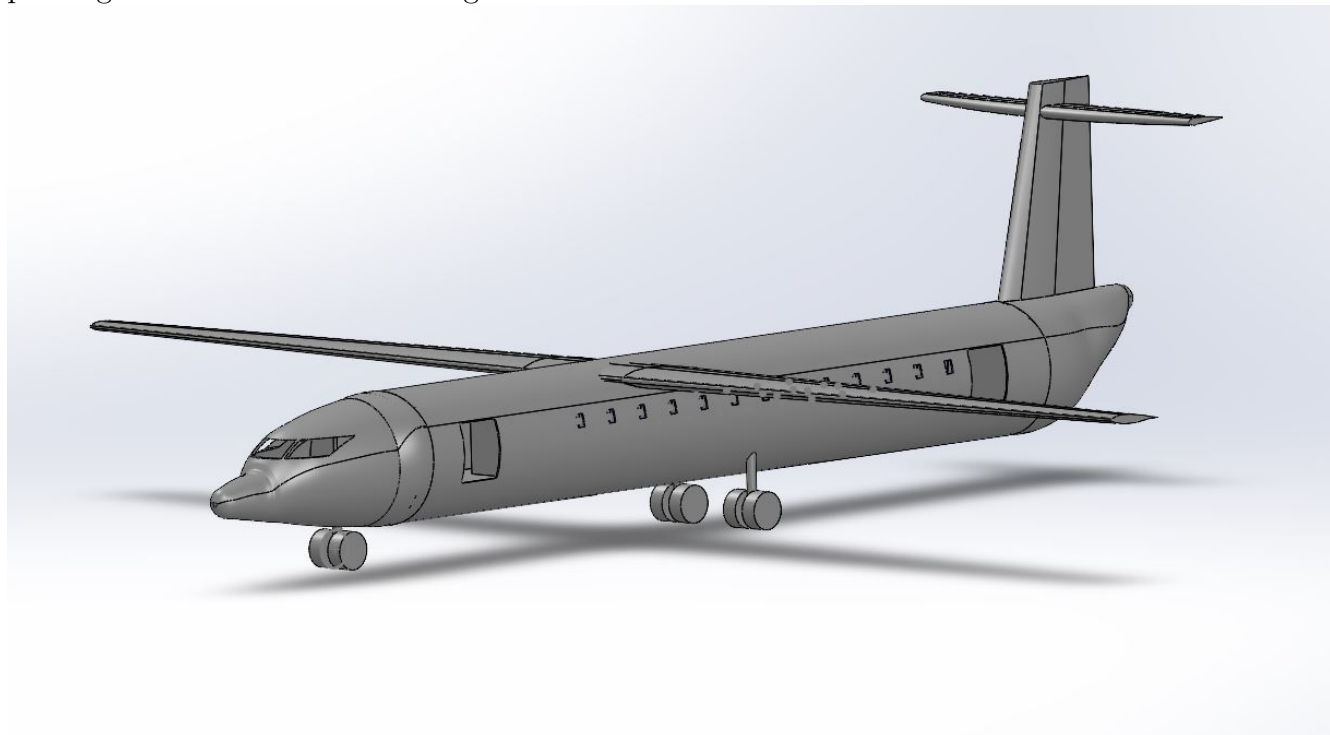


Figure 7.1 – Three-Dimensional View of aircraft

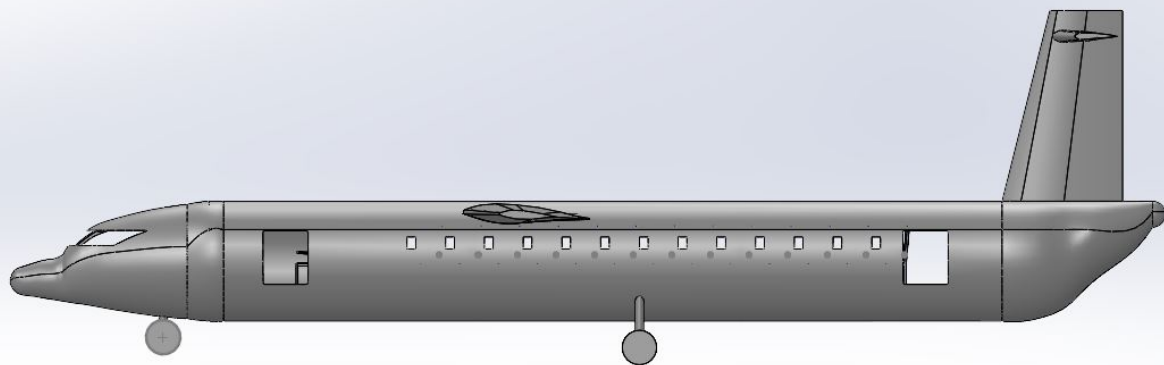


Figure 7.2 – Side view of CAD Model

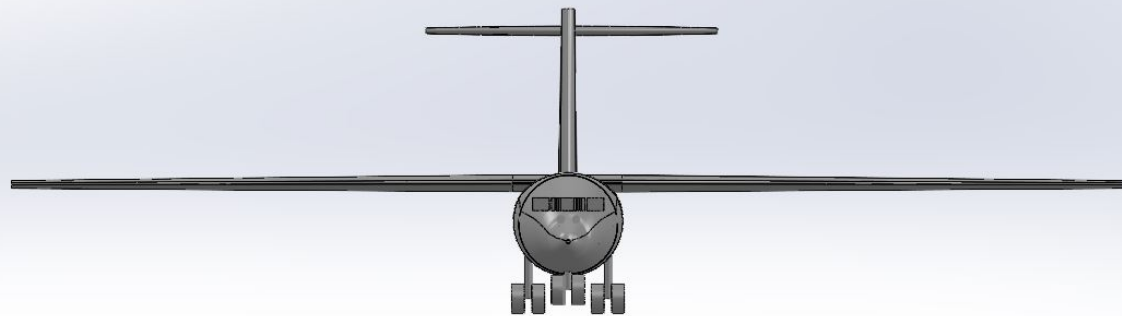


Figure 7.3 – Front view of CAD Model

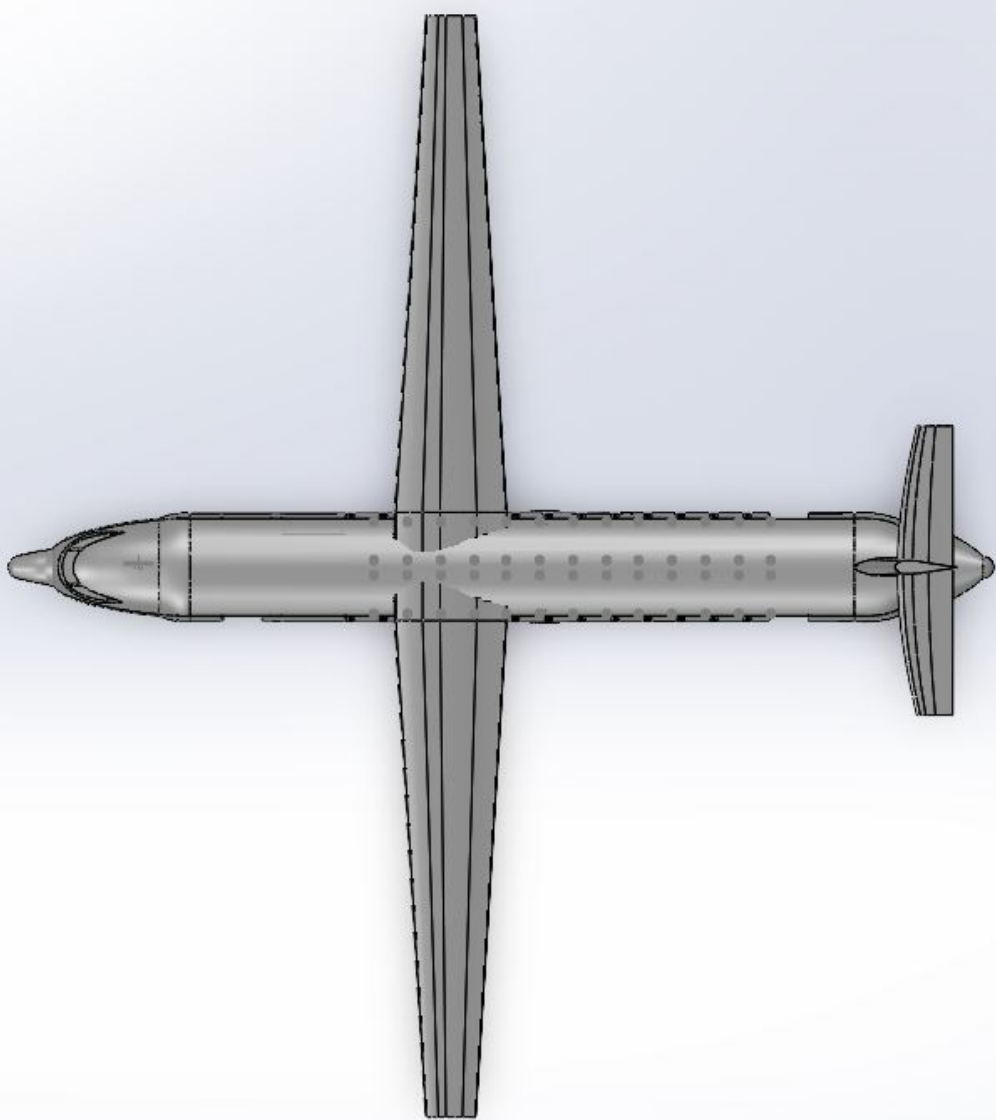


Figure 7.4 – Top view of CAD Model

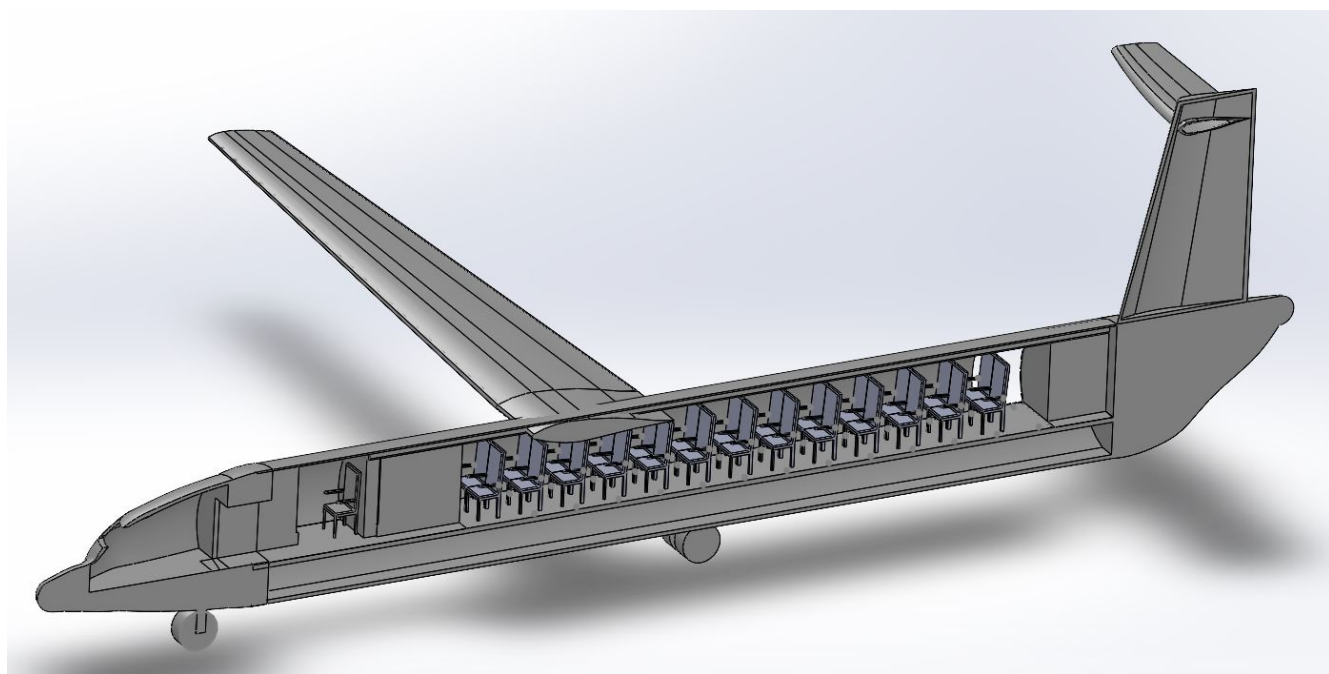


Figure 7.5 – Three-Dimensional view with cut in half along x-z plane

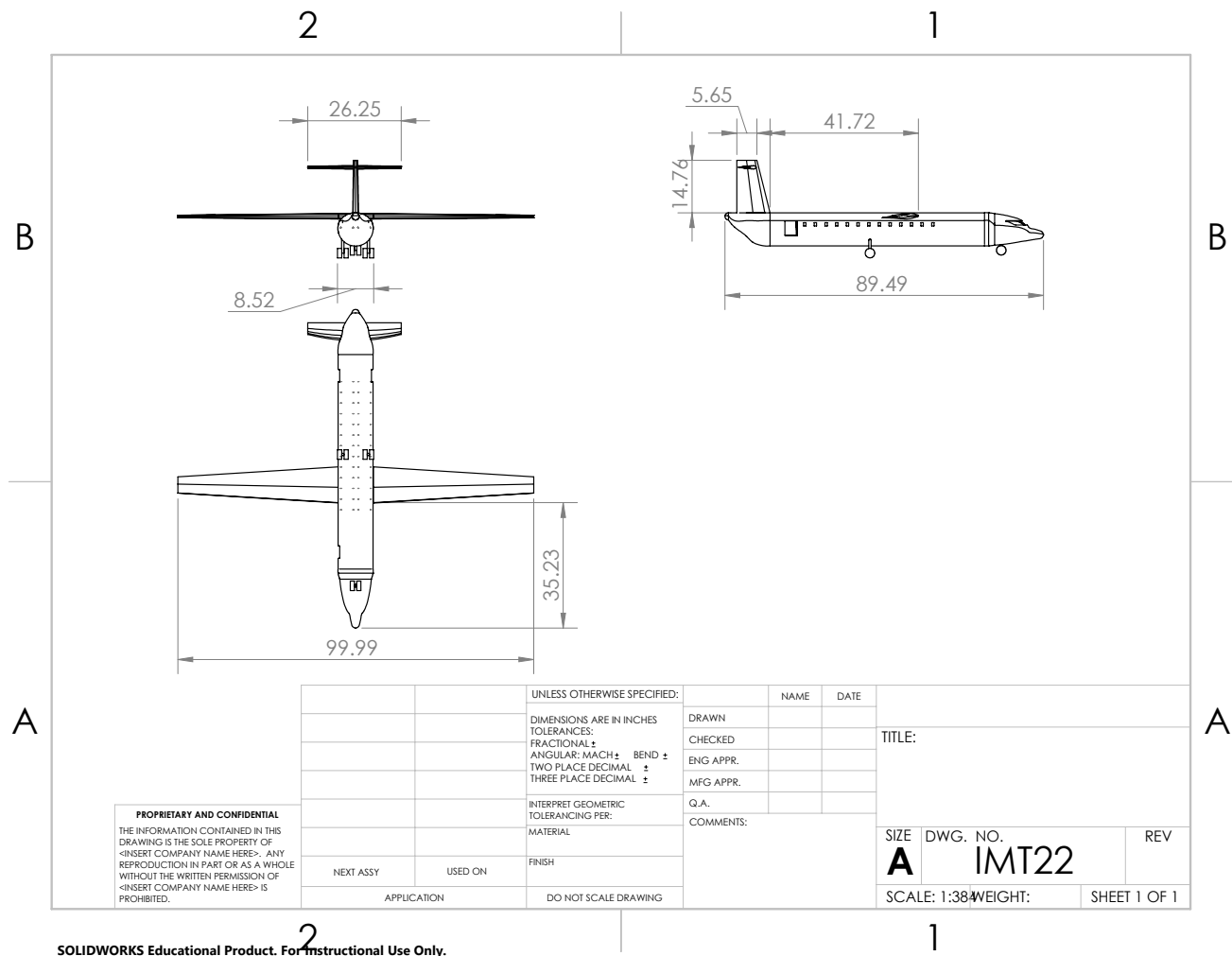


Figure 7.6 – CAD Drawing of Passenger seat arrangement

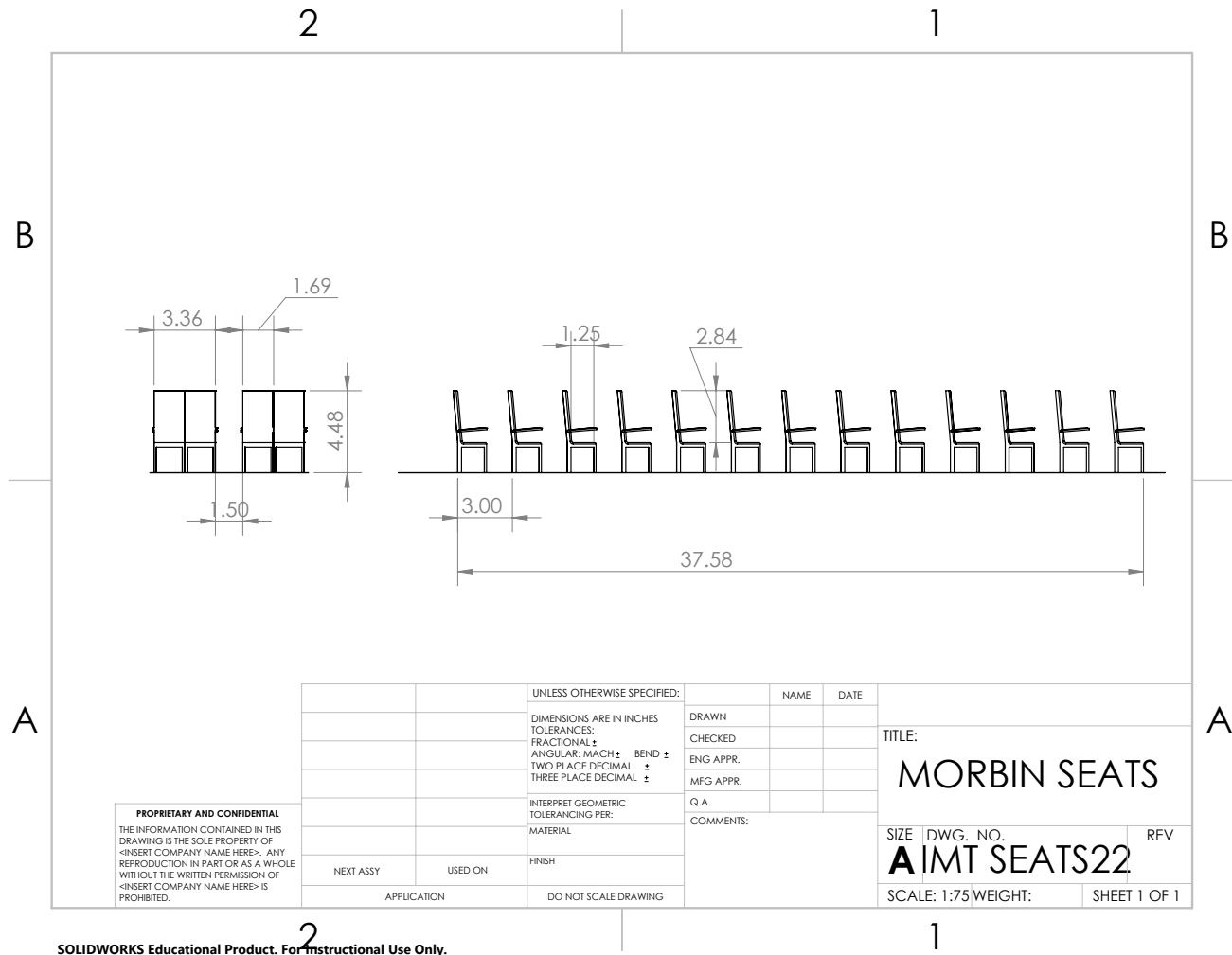


Figure 7.7 – CAD Drawing of Passenger seat arrangement

8 Cost Analysis

The ability of turboprops to operate with a lower carbon footprint is highly exceptional. Still, according to ICCT research [3] these turboprops are an old technology, and their cost were certainly unmatched to today's standard. Which makes it very difficult to adjust the cost to today's standard. Therefore the DAPCA-IV model from Raymer [8] won't be highly accurate unless adjusted for yearly index. For this reason some of the values for the model have been adjusted to reflect the cost estimation for IMT-22 aircraft.

8.1 2022 Adjustments

One of the factors that will be adjusted are the wrap rates. We'll be using the 2021 wrap rate factor for the 2012 values listed in Raymer's book. This factor is shown in Equation 8.1 from

CAVU financial solutions [2].

$$W_{rate}Fudge = (1 + Fringe) * (1 + Overhead) * (1 + GA) = 1.11 \quad (8.1)$$

Another adjustment to be accounted for is the design and fabrication section of the aircraft. Since most of the IMT-22 structure will be made from composite (CFPR), a fudge factor of 1.2 will be used to adjust the DAPCA-IV hours.

Additionally DAPCA tends to over-predict commercial aircraft costs. Instead Raymer advised those can be factored by (0.9-0.25) fudge. So a 0.7 fudge factor is a safe assumption to balance out the offset.

8.2 R&D Cost

The research and development costs are displayed in 8.1. The Avionics accounts for an adjustment of \$10,000 per pound. Additionally the ITM-22 will be equipped with two PW150 engine valued at \$1,300,000 each in present day. Early guesstimates is that about 15 planes to be produced in 5 years.

Table 8.1 – Research and Development Cost

Category	USD
Engineering	\$85,128,938
Tooling	\$36,791,539
Manufacturing	\$6,699,569,760
Quality Control	\$6,380,436
Development Support	\$16,397,164
Flight Test Cost	\$37,378,72
Material Manufacturing Cost	\$883,859,52
Flight Test Control	\$14,837,075
Total Engine Cost (15x2)	\$37,000,000
Avionics	\$109,000,000

8.3 Operation & Maintenance

To determine maintenance and operations cost, we need several other costs. For commercial aircraft (which fly many more hours per year), the fuel totals about 38% of OM costs, the crew salaries about 24%, and the maintenance about 25%. The depreciation of the aircraft purchase price is about 12% of total OM costs, and the insurance is the remaining 1%. Using a script listed in the appendix we get those values listed in the Table below. A 6\$ per gallon fuel cost will be used to estimate the total fuel cost per year.

Table 8.2 – Operational & Maintenance Cost

Category	USD
Fuel cost per year	\$167,076,000
O&M Total	\$439,673,684
Crew	\$105,521,684
Maintenance Cost	\$109,918,421
Depreciation Cost	\$52,760,842
Insurance Cost	43,967,368
Landing Fee	\$87,934,736

8.4 Pricing and Revenue

Based on a historical data planes like (ATR-600, the ITM-22 would sell at starting price of 12,000,000 with a 12% profit margin in present day. Compared to a total cost per plane (R&D and O&M) that is about 4,440,612,777, it's break even point is after selling 37 planes.

9 Conclusion

9.1 Efficiency Merit

As discussed in the Propulsion section, the efficiency target was met and exceeded by 7%. The aircraft is ICAO class C compliant, can carry 54 passengers with luggage including crew, and takes off in under 4500 ft. The plane also exceeds the minimum cruise speed of 275 knots with a cruise speed of 350 knots, in addition to an additional 200 nautical miles of range over the required 1000.

9.2 Conclusion

The IMT22 is a regional turboprop hybrid boasting a 1200 nautical mile range, 52 passenger capacity, and 12660 pounds of passengers or cargo, all while reducing fuel usage by 27% when compared with current turboprop competitors. Further efficiency gains may be found in future analysis through improved battery energy density, advanced composite techniques, and the addition of winglets to maximize the efficiency of the aircraft.

10 Appendix

10.1 Codes and Scripts

10.1.1 Plane Class and Equations

```

P_Wmetric = 8 #KW/kg, 2035
P_W_motor = P_Wmetric * 1.34102 /2.2046
def motorWeights(P_W_motor,hp_req):
    return hp_req / P_W_motor
Tfactor = [motorWeights(P_W_motor,21200)-motorWeights(P_W_motor,28000),0,motorWeights(P_W_
#print(Tfactor)

class Plane:
    def __init__(self, number, T_W, W_S,L_D,SFC,n_hyb,Tfactor):
        self.number = number
        self.T_W = T_W
        self.W_S = W_S
        self.S = 833.35
        self.L_D = L_D
        self.SFC = SFC
        self.n_hyb = n_hyb
        self.w0 = W_S * self.S + Tfactor

    def set_w0(self,w0):
        self.w0 = w0
    def get_w0(self):
        return self.w0
    def get_W_S(self):
        return self.W_S

    def __str__(self):
        return ("Plane " + str(self.number) +", w0 = " + str(self.w0) + ", T_W = " + str(self.T_W) +
               ", W_S = " + str(self.w0/self.S) + ", T0_dist = " + str(self.T0distance()))

    def wf_w0(self):
        KTAS = 350
        wTO = 1
        wClimb = .985

```

```
wCruise1 = Cruise_wFrac(1000-239.2,self.SFC,KTAS,self.L_D)
rangeElec = Range_electric(15,1050,.912,.80,6291,68343*wClimb*wCruise1) * 0.539957
wLoit1 = End_wFrac(0.75,self.SFC,self.L_D*.866) #45 min
wCruise2 = Cruise_wFrac(200,self.SFC,KTAS,self.L_D)
wLoit2 = End_wFrac(0.33333,self.SFC,self.L_D*.866)
wLand = 1
return 1.06 * (1- (wT0*wClimb*wCruise1*wLoit1*wLand*wCruise2*wLoit2)*self.n_hyb)

def we_w0(self):
    if self.w0:
        return 0.912*self.w0**-0.05
    else:
        return "Still need w0!"

def Vstall(self): #USE IMPERIAL, returns ft/s
    return np.sqrt((2*self.w0)/(0.00238*self.S*2.2))
def Vapproach(self):
    return self.Vstall() * 1.3

def T0distance(self):
    denSL = 0.00238
    vStall = self.Vstall()
    mu_r = 0.025
    K = 0.2
    Cl_max = 2.2
    C_d = 0.02
    v_lof = 1.1 * vStall
    v_avg = 0.707 * v_lof
    Cl_opt = mu_r / 2*K
    D_avg = C_d + 2*K*Cl_opt**2
    q_avg = (1/2) * denSL * v_avg**2
    a_avg = (32.2/self.w0) * ((self.T_W*self.w0)-(D_avg*q_avg*self.S)-mu_r*(self.w0-(q_avg
    return ((v_lof**2)/(2*a_avg))
```

10.1.2 Script for Trade Study

```

import numpy as np
import matplotlib.pyplot as plt

#Trade Study: W/S +- 10 and T/W +- 0.05; Constraints: T0_dist < 4500
delta_t_w = [-0.05,0,0.05]
delta_W_S = [-10,0,10]
L_D = 15
SFC = 0.3818
n_hyb = 0.910425
S = 833.35
W_S = 82.01
T_W = 0.205

planes = []
for i in range(len(delta_W_S)):
    for j in range(len(delta_t_w)):
        planes.append(Plane(i*3+j+1,T_W + delta_t_w[j],W_S + delta_W_S[i],L_D,SFC,n_hyb,Tfactor))
Neg_T_W = planes[::3]
Neut_T_W = planes[1::3]
Pos_T_W = planes[2::3]
for i in Neg_T_W:
    print(i.get_w0(),i.T0distance(),(i.Vapproach()*0.592484))
    for i in Neut_T_W:
        print(i.get_w0(),i.T0distance(),(i.Vapproach()*0.592484))
    for i in Pos_T_W:
        print(i.get_w0(),i.T0distance(),(i.Vapproach()*0.592484))

```

List of Figures

2.1	Project Flow	2
2.2	Mission Profile	3
3.1	Aspect Ratio and Wing loading	6
3.2	Design Trade $\frac{T}{W} - \frac{W}{S}$	7
3.3	V-n diagram)	8
4.1	Cl. vs. Cd at design Limit	10
4.2	Cl. vs Alpha	11
4.3	Cl/Cd vs. Alpha	12
5.1	Series Powertrain	14
5.2	Parallel Powertrain	14
5.3	Predicted Energy Density of Battery Types	15
5.4	A Conceptual Distributed Electric Regional Aircraft	18
6.1	XFLR Plane with Masses	20
6.2	Cm vs. Alpha for the Max Takeoff Weight	21
6.3	Cn vs. Beta for the Max Takeoff Weight	22
6.4	Cm vs. Alpha for Empty Weights	23
7.1	Three-Dimensional View of aircraft	25
7.2	Side view of CAD Model	26
7.3	Front view of CAD Model	26
7.4	Top view of CAD Model	27
7.5	Three-Dimensional view with cut in half along x-z plane	28
7.6	CAD Drawing of Passenger seat arrangement	29
7.7	CAD Drawing of Passenger seat arrangement	30

List of Tables

1.1	Team Organization Chart	1
2.1	Specification Requirements	3
2.2	Mission Weight Fractions	4
2.3	Summary of Weights	5
2.4	Baseline Plane Dimensions	5
3.1	Optimization Parameters	7
3.2	Optimal Plane Configuration	8
4.1	Aifoils Considered	9
4.2	Wing Specification	11
4.3	Tail Configuration Matrix	12

4.4	Horizontal Tail	13
4.5	Vertical Tail	13
5.1	Propulsion Selection Matrix	15
5.2	Engine Options	19
6.1	Weights and Balances Sheet	19
7.1	Material Selection	24
8.1	Research and Development Cost	31
8.2	Operational & Maintenance Cost	32

References

- [1] Guillem Moreno Bravo, Nurgeldy Praliyev, and Árpád Veress. “Performance analysis of hybrid electric and distributed propulsion system applied on a light aircraft”. In: *Energy* 214 (2021), p. 118823. ISSN: 0360-5442. DOI: <https://doi.org/10.1016/j.energy.2020.118823>. URL: <https://www.sciencedirect.com/science/article/pii/S0360544220319307>.
- [2] Cavu Cost Financial Solutions. Sept. 2022. URL: <https://cavuadvisors.com/about-us/>.
- [3] Embraer. *Why Embraer Plans To Double Its Turboprop Sales Estimation*. 2021. URL: <https://simpleflying.com/embraer-turboprop-sales-estimation/> (visited on 10/16/2022).
- [4] Martin Hepperle. “Electric Flight - Potential and Limitations”. In: (Oct. 2012).
- [5] MatWeb. *MatWeb Material Property Data*. 2022. URL: <https://www.matweb.com/> (visited on 10/19/2022).
- [6] Pratt and Whitney. *Pratt Whitney Canada Announces Certification of PW127XT-M Regional Turboprop Engine*. 2021. URL: <https://newsroom.prattwhitney.com/2022-08-26-Pratt-Whitney-Canada-Announces-Certification-of-PW127XT-M-Regional-Turboprop-Engine> (visited on 10/16/2022).
- [7] Pratt and Whitney. *PW100/PW150 Series*. 2021. URL: <https://www.pwc.ca/en/products-and-services/products/regional-aviation-engines/pw100-150> (visited on 10/16/2022).
- [8] Daniel Raymer. “Aircraft Design: A Conceptual Approach, Sixth Edition”. In: *Aircraft Design: A Conceptual Approach, Sixth Edition* (2018). DOI: 10.2514/4.104909.
- [9] Pasquale M Sforza. *Commercial Airplane Design Principles - 7.1 Introduction - Knovel*. 2014, p. 598. ISBN: 9780124199538.